

THE FUSING MECHANISM OF NiCr RESISTORS IN  
PROGRAMMABLE READ-ONLY MEMORY DEVICES

by

GEORGE BRIAN KENNEY

Submitted in partial fulfillment of the requirements

for the degrees of

BACHELOR OF SCIENCE

and

MASTER OF SCIENCE

at the

Massachusetts Institute of Technology

June, 1975

Signature of Author .....

Department of Materials Science and Engineering  
MAY 9 1975

Certified by .....

Thesis Supervisor

Accepted by .....

Chairman, Departmental Committee on Graduate Students

Accepted by .....

Chairman, Departmental Committee on Theses



## ABSTRACT

THE FUSING MECHANISM OF NiCr RESISTORS IN  
PROGRAMMABLE READ-ONLY MEMORY DEVICES

by

GEORGE BRIAN KENNEY

Submitted to the Department of Materials Science and Engineering on May 9, 1975, in partial fulfillment of the requirements for the degrees of Bachelor of Science and Master of Science.

A technique has been developed for preparing transmission electron microscope samples of Programmable Read Only Memory devices. This technique incorporates the use of the plasma etcher and mechanical polishing techniques to thin the integrated circuit chip to approximately 2500 Angstroms. The plasma etcher is used because it offers a controlled method for uniformly removing very thin layers of silicon and silicon dioxide.

Using these samples, high resolution micrographs were obtained of the nichrome resistors or "fusible links" which make up the memory matrix. Data from these micrographs of the fused region of the nichrome resistors was then used to develop a theory for this fusing mechanism.

This theoretical fusing mechanism of nichrome resistors is based on the theories of Lord Rayleigh concerning the instability of liquid jets and sheets. Prior to melting the narrow section of the thin-film resistor by Joule heating, voids nucleate at triple points by an electromigration mechanism. After the resistors melt, these voids become unstable holes in the thin molten films. As a hole grows and the film begins to pull back, perturbations with a characteristic wavelength develop as predicted by Lord Rayleigh. These perturbations lead to the final break-up to the film in the molten gap region of the resistor. The gap region is then left with a characteristic structure which is different for each type of resistor geometry examined.

Thesis Supervisor: Robert E. Ogilvie  
Title: Professor of Materials Science

## Table of Contents

<u>Section No.</u>		<u>Page No.</u>
	Abstract	2
	List of Figures	5
	List of Tables	7
	Acknowledgments	8
I	Introduction	9
II	Literature Survey	11
	A. Previous Studies of NiCr Resistors	11
	B. Previous Studies of NiCr Resistors used in PROM Devices	13
	C. Liquid Jet and Sheet Instability	14
	D. Electromigration	16
III	The Theory of Liquid Jet and Sheet Instability	17
	A. The Rayleigh Jet	17
	B. Thin Fluid Film Instability	21
	1. The Formation of Liquid Threads or Fingers	22
	2. The Presence and Effects of Holes	24
	C. The Theoretical Fusing Mechanism of NiCr Resistors in PROM Devices	26
IV	Materials Preparation and Experimental Procedures	36
	A. Introduction	36
	B. Sample Preparation	36

<u>Section No.</u>		<u>Page No.</u>
	C. Observations and Measurements	39
	1. Forward	39
	2. Transmission Electron Microscope Analysis	39
	3. Scanning Transmission Electron Microscope Analysis	44
	4. Analysis of Micro-micro Electron Diffraction Patterns	45
V	Discussion of Results	58
VI	Summary and Conclusions	61
VII	Suggestions for Future Work	63
VIII	Appendices	64
	I. Sample Preparation	64
	II. Symbols	69
IX	Bibliography	72

## List of Figures

<u>Figure No.</u>		<u>Page No.</u>
1	Illustration of the basic design of the NiCr resistor.	27
2	Illustration of current crowding and hole growth direction.	32
3	A sketch of the basic components of the PROM.	37
4	A schematic of the complete plasma etching apparatus.	67
5a	Illustration of the position of the sample prior to mechanical polishing to partially remove the silicon.	68
5b	Schematic illustration of the initial and final thickness of the sample, where the dotted lines outline the final thickness.	68
6	Low magnification micrograph of the resistor matrix, X450.	40
7	Unblown resistors of: a) Type A, b) Type B.	47
8	Illustration of the heat-affected zone associated with the molten zone or gap region of the Type A resistor, X21,000.	48
9	Gap region of fused Type A resistor, X26,000.	49
10	Higher magnification of Figure 9, X66,000.	50
11	Gap region of fused Type A resistor, X26,000.	51
12	Higher magnification of Figure 11. Illustrates periodic spacing between the fingers, X66,000.	52
13	Gap region of fused, Type B resistor, X21,000.	53
14	Higher magnification of Figure 13, X43,000.	54

<u>Figure No.</u>		<u>Page No.</u>
15	Gap region of another fused, Type B resistor, X21,000.	55
16	Micro-micro diffraction patterns of grey phase in Type A gap region.	57

## List of Tables

<u>Table No.</u>		<u>Page No.</u>
1	Measured values of: $\lambda'$ = spacing between fingers. $\lambda$ = wavelength of perturbation along surface of finger.  Calculated values of standard deviation and variance.	56
2	Measured values of: $\delta$ = the spacing between the spherical particles.	56
3	Values of variables used.	71

## Acknowledgements

The author would like to express his gratitude and sincere appreciation to the following persons who have contributed much time and effort over the past year.

To my advisor, Professor Robert Ogilvie, for his thoughtful guidance and continual stimulation.

To Al Williams, for his assistance in preparing the drawn figures.

To the Computer and Special Test Equipment Division of Charles Stark Draper Laboratory, Inc., for financial support and continued technical assistance. Special thanks to Dr. W. Kinzy Jones for his continual assistance and helpful suggestions and to Anthony M. Marques, for his invaluable technical advice.

To my parents and grandparents for their support and encouragement over the past five years.

Above all, to my wife Nancy, for her constant patience and devotion during the past year.



## I. INTRODUCTION

The purpose of this investigation is to study and subsequently develop a theory for the fusing mechanism of nichrome resistors in Programmable Read Only Memory (PROM) devices. This fusing process is important because it in itself can determine the reliability of these integrated circuit memory devices.

These PROM devices, which are used in everything from simple hand held calculators to sophisticated guidance computers, consist basically of a 2 dimensional matrix of nichrome resistors. These devices function in an analogous fashion to ferrite core memory, in that, the resistors in this known matrix can be fused or blown in a specific pattern to introduce the binary code used by computers. In the binary code, an open circuit or fused resistor corresponds to a 0 while a closed circuit or unfused resistor corresponds to a 1. A resistor is fused by pulsing an excessive amount of current through it. This causes it to melt and open the circuit by pulling back to form a gap in a manner similar to how a household electrical fuse blows. Therefore, the formation of a clean gap, across which no current can flow, is critical to the reliability of the device.

In order to examine the gap region, a technique had to be developed for preparing transmission electron microscope samples of the PROM devices (1). With these samples high resolution micrographs of the resistor gap region can be obtained.

A theory is developed which attempts to explain the fusing mechanism of the nichrome resistors. This theory is based on the theories of Lord Rayleigh which deal with the instability of fluid jets and sheets. The proposed theory, as a first step, discusses the nucleation of voids at triple points in the narrow region of the resistor. This occurs prior to the melting of the gap region by Joule heating. Upon melting the voids become unstable holes in the thin molten film. As these holes grow, perturbations develop with a characteristic wavelength as predicted by Lord Rayleigh. As these perturbations grow, the thin molten film breaks up leaving a characteristic structure in the gap region as observed in the transmission electron micrographs.

Observations and measurements made from these micrographs are in good agreement with calculated values of the perturbation wavelengths. Micro-micro diffraction patterns obtained from a 200 kilovolt transmission electron microscope and data collected using the scanning transmission electron microscope is also used to support the proposed theory.

## II. LITERATURE SURVEY

## A. Previous Studies on Nickel-Chromium Resistors.

Nickel-chromium (NiCr) thin film resistors, with their very low temperature coefficients of resistance and immunity to ionizing radiation, are used extensively in radiation hardened integrated circuits. Because of this application and the consequential demand for high reliability, a considerable effort has been made to study and better understand the nature of the resistor.

Fabrication techniques of thin films are covered extensively in the literature (2, 3, 4). This includes the nucleation, growth and structure of films in general.

The structure of vacuum deposited NiCr films has been reported by several authors (5, 6, 7). Taylor and Floyd (7) have presented a very useful table of compositions, lattice parameters and structures of NiCr binary alloys. Bicknell, et al. (5) vacuum deposited thin films of NiCr on to the surface of cleaved rock salt and found the films to consist of a dispersion of islands. However, Philofsky, et al. (8) report that 150 Angstrom thick NiCr films deposited on silicon dioxide are continuous and void-free. Philofsky suggests that the discrepancy can be attributed to the different surface structures of the silicon dioxide and rock salt and the reaction between these substrates and the evaporating NiCr. The phase diagram for the NiCr system is also reported by Hansen (9).

Lakshmanan (10) studied some of the basic properties of thin NiCr films and found the resistance to be very stable. The major factors

thought to affect the stability of NiCr thin film resistors, such as annealing temperature, manufacturing processes, form factors, power density and trimming, have been evaluated by Ahern and Heid (11). They report that the annealing temperature is the only real control one has on stability.

The reliability of NiCr resistors has been studied and reported in the literature (8, 12, 13). 150 Angstroms thick NiCr resistors are reported to function with a high degree of reliability when operated within well defined power levels. The resistors are also immune to failures due to power cycling at high current densities and thermo-mechanical fatigue (8). In any discussion of reliability, reproducibility must also be considered. Nagata, et al. (14) have reported very favorable results concerning the reproducibility of NiCr thin-film resistors when using an in-line deposition system.

Properly fabricated and treated NiCr resistors can deliver reliable service for remarkable periods of time. However, because they are so thin, they are very susceptible to damage if not used according to the manufacturers specifications. Keenan, et al. (15) have summarized the various possible modes of failure. They report that while failures due to electromigration and voltage overstress are functions of the ratio of operating specifications and actual operating conditions, other failure modes have been attributed to the temperatures and environments to which the resistors have been exposed.

It is this curious combination of good reliability and high susceptibility to damage that has led to extensive studies on this NiCr thin-

film resistor.

#### B. Previous Studies on NiCr Resistors Used in PROM Devices.

As previously stated, PROM devices consist basically of a 2 dimensional matrix of NiCr resistors. These resistors are then blown in a specific pattern to introduce the binary code used by computers. Therefore, the reliability of the NiCr resistors or fuses in this application may be treated in two parts. Specifically, the reliability of both the blown and unblown resistors must be investigated.

The reliability of the unblown resistors, as discussed in the previous section, has been reported as excellent when the resistors are properly fabricated and operated within well defined specifications.

The reliability of blown resistors is directly related to the probability of a "healing" or growback mechanism occurring (16). However, this failure mechanism can be minimized by fusing the resistors under proper blowing conditions. Therefore, having established the reliability of both the blown and unblown resistors, PROM devices can be used with confidence.

Although the reliability of the fused NiCr resistor has been established, its fusing mechanism is not. This is due, in part, to the size of the individual resistors and the time constant associated with the fusing mechanism. Therefore, the first logical step in studying this mechanism is to examine the resistor before and after it is fused. However, to do this the resistor has to be examined using an electron microscope because optical techniques lack the resolution required to illustrate the

fine features of the gap region of a fused resistor. Therefore, a technique had to be developed for preparing a PROM device, with its NiCr resistors, for observation in the scanning and transmission electron microscope. Devaney (17) has developed such a technique for preparing the PROM device for scanning electron microscopy studies. However, Jones (1) has developed a technique for preparing PROM devices for studies in both the transmission and scanning electron microscope. Both use a plasma etching procedure.

### C. Liquid Jet and Sheet Instability

Liquid jet disintegration has been subject to theoretical and experimental investigation for the past hundred years, the first analysis being reported by Lord Rayleigh in 1879 (19). In this first treatment Rayleigh considered only the effect of the capillary force. He assumed that a disturbance with a characteristic wavelength existed on the surface of the cylinder and then proceeded to calculate the value of this wavelength based on energy considerations. He concluded that the minimum wavelength necessary to render the cylinder unstable was equal to  $\pi$  times the diameter of the cylinder. A value for the ratio of wavelength to diameter for the perturbation leading most rapidly to the disintegration of a cylindrical jet was also derived. In subsequent reports (20, 21), Rayleigh has confirmed these initial findings.

Lamb (22) has also considered the problem of jet disintegration based on a method of velocity potential. This work also serves to confirm the original calculations made by Rayleigh.

Rayleigh also attempted to account for the effect of viscosity on the disintegration of liquid jets (23). However, it was not until 1931, when Weber (24) reported his theoretical analysis of liquid jet disintegration, that the effect of viscosity was properly accounted for.

A good review of the work of Rayleigh, Weber and others on jet disintegration is given by Miesse (25) as he attempts to correlate these theories with experimental data. Brodkey (26) has also presented a good review of the mechanisms of jet, sheet and bubble disintegration. Using stroboscopic techniques, excellent photographs of the different disintegration mechanisms were obtained.

Dombrowski and Fraser (27) conducted a photographic investigation of the disintegration of liquid sheets. Single-hole, fan-spray nozzles were used to produce the sheets which were then photographed using a micro-second light flash source.

The independent effects of surface tension, viscosity and density were evaluated. It is reported that liquid sheets with high viscosity and surface tension will be most resistant to disintegration, with density having no effect at all. It is also reported that unwettable particles puncture and perforate the sheet.

Fraser (28) has reported on the properties of perforations or holes in spray sheets. The initiation of the holes is considered and an expression describing its rate of growth has been derived from a force balance.

The holes are usually attributed to the presence of unwettable particles held in solution. However, a sheet of a pure, homogeneous liquid flowing under vacuum is also punctured by holes. Fraser, does not satisfactorily explain this phenomenon.

#### D. Electromigration

Electromigration is a transport phenomenon induced by high dc current densities and has been observed for several decades. In such a system, thermally activated metal ions are acted upon by two opposing forces (29). The force of the electric field, acting in the direction opposite to the electron flow, has little effect because of the shielding electrons around the metal ions. The predominant force is that due to the "electron wind" which is the result of the rate of momentum exchange between the conducting electrons and the activated metal ions. This gives rise to an atom flux in the direction of electron flow and a vacancy flux in the opposite direction. This is in agreement with the theory of current-induced mass transport developed by Huntington and Grone (31).

It is also reported that electromigration occurs primarily along the grain boundaries (31, 32, 33) where the activation energy is lowest.

Rosenberg and Ohring (34) report that hole formation is due to a two step process of void nucleation which is essentially instantaneous and void grow by an accumulation of vacancies. The latter step requires extensive incubation periods and occurs preferentially at triple points.

It is the growth of voids at regions of ion flux divergence that leads to the formation of large holes in conductors. Such regions of ion flux divergence correspond to temperature and current density gradients (35, 36). At such locations, atoms migrate up the gradients. That is, atoms leave their positions to move up the gradient at a faster rate than they can be replaced by atoms moving into these positions from the regions of lower or nonexistent gradients.



### III. The Theory of Liquid Jet and Sheet Instability

#### A. The Rayleigh Jet

The first of the theoretical analyses of jet disintegration were presented by Lord Rayleigh (19, 20, 21) and he states that, "It consists in the operation of the capillary force, whose effect is to render the infinite cylinder an unstable form of equilibrium, and to favor its disintegration into detached masses whose aggregate surface is less than that of the cylinder." In this derivation Rayleigh has assumed axial symmetry and irrotational flow as applied to a nonviscous liquid.

Perturbations of all wavelengths ( $\lambda$ ) are possible on the surface of the jet. However, one perturbation, with a wavelength characteristic of the liquid used, will predominate. Since the growth rate is exponential with time, this perturbation will grow more quickly than the others and will be the only one observed.

The various perturbations, growing exponentially with time ( $t$ ) can be represented by

$$\alpha_1 e^{q_1 t}, \alpha_2 e^{q_2 t}, \alpha_3 e^{q_3 t}, \dots$$

where  $\alpha$  represents the perturbations initially and  $q_1 > q_2 > q_3 \dots$ . If  $\alpha_1$  and  $\alpha_2$  are initially very small, then the perturbation with the fastest growth rate,  $q_1$ , will predominate. For example, consider the ratio of the two strongest perturbations

$$\alpha_2 e^{q_2 t} / \alpha_1 e^{q_1 t} = (\alpha_2 / \alpha_1) e^{-(q_1 - q_2)t}$$

As  $t$  increases both expressions go to zero. Therefore, the predominant perturbation which develops on the jet will have the wavelength corresponding to the fastest growth rate.

Having determined that one perturbation or wave, with a specific wavelength, will predominate on the surface of the jet, Rayleigh then calculated the value of this wavelength. To do this, he first derived expressions for the potential and kinetic energies of the system and then using Lagrange's method of variation of parameters derived an expression for the "growth rate" ( $q$ ) of the waves.

In order for a perturbation of any wavelength to develop on the surface of the jet, it must decrease the total energy or surface area of the system. The potential energy ( $V$ ) of the system is given as surface area ( $\sigma$ ) times the surface tension ( $\gamma$ ).

To calculate the potential energy change due to the presence of the perturbation, Rayleigh began with the following equation for the surface of the cylinder:

$$r = a + \alpha \cos k Z$$

$r$  is the radius of a cylinder with  $Z$  taken along its axis.  $k = 2\pi/\lambda$  and  $a$  is a variable value of the radius. With this equation, Rayleigh derived the following expression for the change in surface area per unit length (per unit wavelength) of the cylinder due to the presence of the perturbation:

$$\sigma - \sigma_0 = \frac{\pi \alpha^2}{2a} (k^2 a^2 - 1)$$

$\sigma = \sigma_0$  for the case when no perturbations exist on the surface of the cylinder.

Therefore, the potential energy due to the change in surface area

$$V = -\gamma \left[ \frac{\pi \alpha^2}{2a} (1 - k^2 a^2) \right]$$

is negative if  $ka < 1$  and positive if  $ka > 1$ . Thus, if  $ka > 1$  or  $\lambda < 2\pi a$ , the surface area or total energy of the system is increased by the perturbation. This is energetically unfavorable and so the surface is stable. Therefore,  $\lambda = 2\pi a$  is the minimum wavelength which can render the surface of the cylinder unstable.

To calculate the kinetic energy (T), Rayleigh used the following expression for the velocity potential ( $\phi$ )

$$\phi = A J_0(ikr) \cos kZ$$

where  $J_0$  represents a Bessel function of zero order and A is a coefficient.

Denoting the density as  $\rho$  and considering a unit length (wavelength) of the cylinder, the following expression is determined for the kinetic energy:

$$T = \frac{1}{2} \rho \pi a^2 \left[ \frac{J_0(ika) \dot{\alpha}^2}{(ika) J_0'(ika)} \right]$$

With  $\alpha \propto e^{qt}$  and using Lagrange's method of variation of parameters, an expression is determined for the growth rate of the waves:

$$q^2 = \frac{\gamma}{\rho a^3} \left[ \frac{(1 - k^2 a^2) (ika) (J_0'(ika))}{J_0(ika)} \right]$$

This equation determines the growth rate of perturbations for wavelength  $\lambda$ . However,  $q^2$  is given as a function of  $ka$  and therefore, there must exist a value of  $ka$  which maximizes  $q^2$ . Expanding

$$\frac{(1-k^2 a^2)(ika)(J'_0(ika))}{J_0(ika)}$$

and solving the quadratic for  $k^2 a^2$  gives:

$$ka = .6970$$

or

$$\lambda = 4.508 \quad (2a)$$

This is the value of the wavelength for the perturbation which leads most rapidly to the disintegration of the cylindrical mass.

In a later paper (23), Rayleigh considered the effect of viscosity on the disintegration of a liquid jet. Initially, he had considered only the effect of the capillary forces. This analysis resulted in a complicated expression for  $q$ . However, from the expression, he was able to predict that a viscous liquid would have perturbations with large wavelengths.

Weber (24) also reported on the theoretical analyses of liquid jet disintegration. He considered the combined effects of viscosity and capillary force and obtained the same complicated expression for  $q$  as derived by Rayleigh. However, for  $ka < 1$ , Weber was able to simplify this expression and solving for the value of  $ka$  which maximizes  $q$

obtained

$$\lambda = 2\pi a [2(3Z + 1)]^{1/2}$$

where

$$Z = W/R$$

and

$$W = \text{Weber number} = U (2\rho a/\gamma)^{1/2}$$

$$R = \text{Reynolds number} = 2U\rho a/\eta$$

$U$  is the velocity of the jet and  $\eta$  is the coefficient of dynamic viscosity. From this it is seen that for non-viscous liquids ( $Z = 0$ ),  $\lambda = 4.44 (2a)$  and for viscous liquids ( $Z \rightarrow \infty$ ),  $\lambda \rightarrow \infty$ . This is in agreement with the earlier work of Lord Rayleigh.

#### B. Thin Fluid Film Instability

The purpose of Dombrowski's investigation (26) was to study the effect of liquid properties on the development and stability of liquid sheets. The surface tension, viscosity and density were considered to be the major contributors to the disruption of the spray sheets.

To study the independent effects of surface tension, viscosity and density on the stability of thin sheets, Dombrowski sprayed a selection of liquids into air. All of the liquids were sprayed at a constant liquid-to-air velocity. For example, to study the independent effect of surface tension, several liquids with approximately the same viscosity and density but increasing surface tension are sprayed, photographed and compared. Since only the surface tension of each liquid is changing,

all changes observed in the photographs are attributed to surface tension.

Surface tension, independent of all other properties, was found to have a profound effect upon the stability of the spray sheet. An increase in the surface tension leads to a reduction in the overall sheet surface area but also results in a larger perturbation-free zone. Therefore, the stability of the sheet is increased by an increase in surface tension.

The independent effect of viscosity is very similar to that of surface tension with one specific difference. Sheet stability also increases with viscosity, however, the surface area of the sheet also increases in contrast to the effect of surface tension. These sheets with high viscosity are also found to have undisturbed rims. This behavior has been predicted by Weber (24) who showed that as viscosity increases, the rate of growth of perturbations decreases.

No real stabilizing effect can be attributed to changes in density. However, the combined effect of increasing density and surface tension results in a very stable sheet which is devoid of major waves.

#### 1. The Formation of Liquid Threads or Fingers

Two opposing forces are at work in the liquid sheet. The inertia or expansion force results in giving the particles in the sheet a radial velocity. The opposing force of surface tension imparts a velocity of contraction to the particles in the sheet. If the surface tension were zero, all of the particles would move out radially in the fan. However, since the surface tension is non-zero the particles follow a curved path inwards toward the axis of the sheet. Since the edge of a liquid sheet is subjected to unbalanced surface forces, it

contracts instantaneously forming a thick cylindrical rim. This rim is analogous to a cylinder of liquid and therefore obeys the same rules for disintegration as specified by Rayleigh (19). Since the wavelength of the perturbation on the surface of the cylinder is a function of surface tension, it is therefore the surface tension that leads to the disintegration of the edge of the sheet with the same wavelength as found on cylinders of the same liquid.

Dombrowski states that "In the disintegration of a sheet of liquid the formation of ligaments or threads is a necessary stage before the production of drops." He has also found that threads can be formed at any free edge or new boundary such as the edge of a hole produced by a perforation in the film.

Therefore, a perturbation (with its characteristic wavelength) which forms on the cylindrical rim grows into a drop, as it is centrifuged radially outward or as the cylindrical rim rolls or pulls back towards the axis of the sheet. Thus, as the rim is pulled in, the drop is left behind and necks out from the rim leaving a thread between itself and the rim. This thread eventually breaks up because it is a cylinder of liquid itself and subject to Rayleigh's laws of disintegration based on surface tension. Therefore, a series of spherical particles of various sizes is produced by the disintegration of the free edge of the sheet or periphery of a hole.

## 2. The Presence and Effects of Holes

Dombrowski has defined the stability of a liquid as "its resistance to disintegration." The major factors controlling the stability of thin sheets are surface tension, as previously discussed, and suspensions in the liquid.

The stability of thin liquid films has been found to be strongly dependent upon the type of solid or liquid particles held in suspension. Dombrowski found that if the solid or liquid particles were wetted by the liquid of the film, they would have no effect on the mode of disintegration of the film. This result was found irrespective of their size. However, for suspended solid and liquid particles which are not wetted by the liquid, the effect is quite devastating. These particles, with sizes on the order of the thickness of the film or larger, form unstable holes or perforations in the film.

These holes are unstable and grow because a hole with a diameter greater than the thickness of the film decreases the surface area of the film (27). Therefore, this is an energetically favorable process because it lowers the total energy of the system.

This result can also be obtained by considering the pressure difference across the boundary of the hole. Blakely (29) shows that

$$\Delta P = \frac{2\gamma}{r} = \gamma(K_1 + K_2)$$

where

$$K_1 = 2/t \quad \text{and} \quad K_2 = -2/d$$



Therefore,

$$\Delta P = 2\gamma \left( \frac{1}{t} - \frac{1}{d} \right)$$

From this equation it is easily seen that  $\Delta P$  is positive if  $d > t$ . Therefore, for  $d > t$ ,  $\Delta P$  is positive and the hole grows. The inverse is true for  $d < t$ , that is,  $\Delta P$  is negative and the hole shrinks and disappears.

As the hole grows, the edge of the sheet around it pulls back and thickens forming a cylindrical rim. This rim also obeys the rules for disintegration as previously discussed.

Fraser (28) has reported on the forces acting on a hole in a thin liquid sheet and has derived an expression for the growth rate of these holes ( $\dot{e}$ ). Equating the surface tension force,  $4\pi r\gamma$ , with the rate of change of momentum, he obtains the following equation:

$$4\pi r\gamma = \frac{d}{dt} [\rho_L \pi r^2 h \dot{e}]$$

where  $h$  is the thickness and  $\rho_L$  is the density of the liquid. Setting  $G = 4\gamma/h\rho_L$  and differentiating, the following equation results:

$$G = e r \frac{de}{dt} + 2e^2$$

After integrating and solving for the boundary conditions, the final expression for the growth rate of the hole is obtained as:

$$\dot{e} = \left[ \frac{G}{2} \right]^{1/2} = \left[ \frac{2\gamma}{h\rho_L} \right]^{1/2}$$

Thus, the growth rate is found to be independent of the radius of the hole. The validity of this equation has been confirmed by experiment.

### C. The Theoretical Fusing Mechanism of NiCr Resistors in PROM Devices

NiCr resistors are fabricated using a vapor deposition technique. These resistors, which are approximately 150 Angstroms thick, are continuous and void free when deposited on thermal oxide. The NiCr resistors of commercially available PROM devices are sandwiched between a layer of passivation and thermal oxide. Therefore, the resistor can be considered to be a thin sheet surrounded by a homogeneous glass phase.

The NiCr resistor is fused or blown by pulsing an excessive amount of current through it to the emitter base. (See Figure 1). This pulse is generated by rapidly building up a positive potential on the bus bar. A ramp rate on the order of 10 volts per micro-second is used to build up this potential to a sufficient level where it is then held for a short period before being ramped down.

The resistor fuses during the initial period when the potential is still rising. That is, the output current of the resistor rises rapidly as the potential is being ramped to its plateau value. Before this value is obtained the resistor output current becomes unstable and quickly falls off to essentially zero. The time necessary for the output current to go through this cycle or for the resistor to fuse is less than 1 micro-second. During this period the resistor, due to Joule heating in its narrow region, has melted and opened a gap in the circuit.

The following sequence of effects, the sum of which must occur in less than 1 micro-second, is offered as an analysis of the fusing mechanism of NiCr resistors.

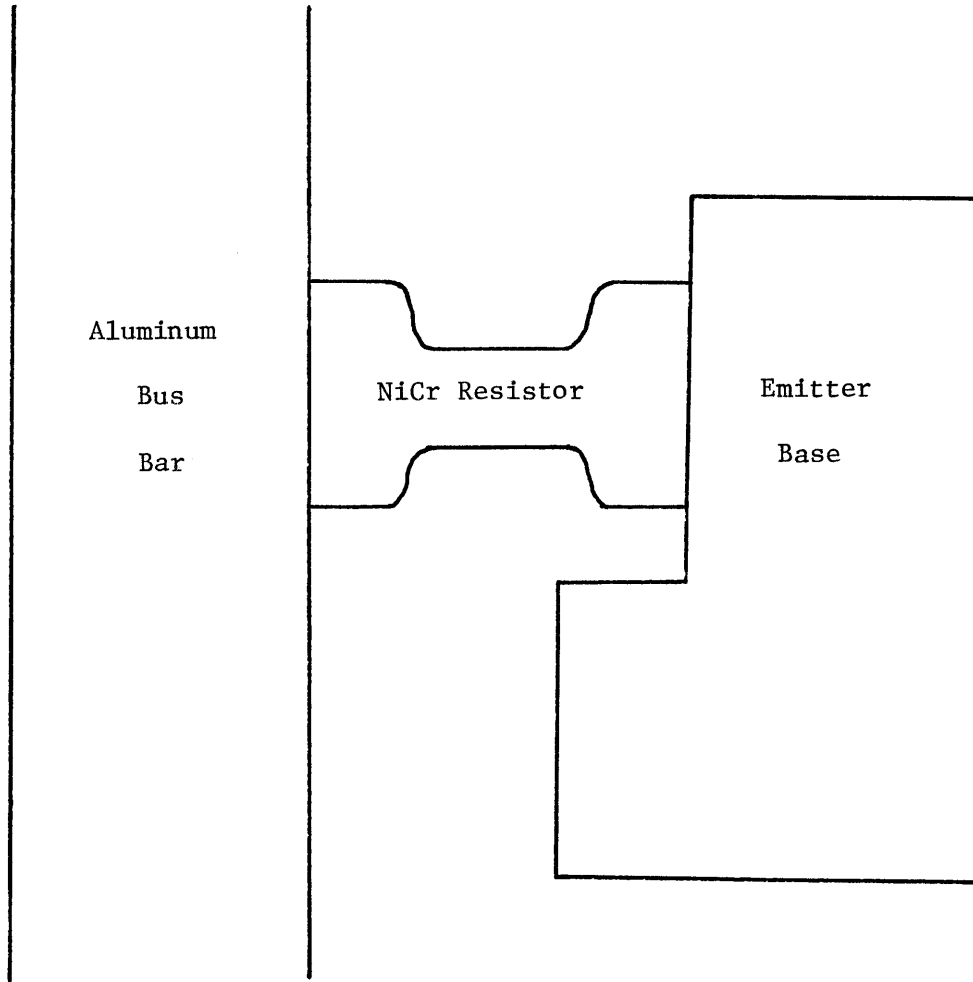


Figure 1: Illustration of the basic design of the NiCr resistor.

The resistor is considered to be a thin sheet surrounded by a uniform glass phase. In order for this sheet to break up in less than 1 microsecond, it must melt and disintegrate by some mechanism of hole growth. This necessitates the formation of a hole in the original void-free sheet either prior to melting or immediately thereafter. This hole must have a diameter greater than the thickness of the sheet. As previously discussed, such a hole in a liquid sheet is unstable and grows.

Such a hole could be formed just prior to melting by an electromigration process. Rosenberg and Ohring (34) have reported that hole formation is due to void nucleation and subsequent void growth through the accumulation of vacancies. This latter step has been reported to require hours to form a hole through thick conductors.

In considering only void nucleation, vacancy supersaturation must be discussed. It is reported (34, 37) that vacancy buildup will take place most rapidly where a maximum in ionic flux divergence occurs. Triple points are ideal locations for this to occur. For an ideally positioned triple point, metal ions will migrate out along 2 grain boundaries in the direction of electron flow while they arrive at the triple point along only 1 grain boundary.

As an order-of-magnitude calculation, in considering the nucleation of a spherical void at a triple point, Rosenberg and Ohring (34) used the following equation:

$$\Delta G = \frac{4\pi r^3}{3\Omega} \Delta U + 4\pi r^2 \gamma_s - \frac{3}{2} \pi r^2 \gamma_b$$

where  $\Delta U$  is the energy gained per vacancy on condensation,  $\Omega$  is the atomic volume,  $\gamma_s$  is the surface energy of the void-metal interface,  $\gamma_b$  is the grain boundary energy and  $\Delta G$ , is the free energy change. The critical radius of the void ( $r^*$ ) is obtained by setting

$$d\Delta G/dr = 0$$

which gives

$$r^* = (8\gamma_s - 3\gamma_b)\Omega/4\Delta U$$

and letting  $\gamma_b \approx \gamma_s/3$  for  $S < 1$  and  $\Delta U = kT \ln(1+S)$  results in

$$r^* = 5.07(10^{-10})\gamma_s/\ln(1+S)$$

where  $S$  is the vacancy supersaturation.

The sheet or NiCr resistor under investigation contains many triple points which extend through the sheet since the grain size and sheet thickness are approximately equal. Therefore, during the current pulse, void formation by electromigration is quite possible. Solving  $r^*$  for NiCr, assuming  $\gamma_s \approx 30$  ergs/cm and  $S \approx .1$ , which is realistic for high temperature, the following result is obtained:

$$r^* \approx 16 \text{ \AA}$$

The values of  $\gamma_s$  and  $S$  used are based on the assumption that similar values exist for NiCr and aluminum at the same normalized temperature.

Although this calculated value of the critical radius of the void is too small to form an unstable hole in the sheet, electromigration as a possible mechanism for hole production prior to melting cannot be

disregarded. The uncertainties in the values of the  $\gamma_s$  and  $S$  used leave room for a large error in the calculated value. Also, no realistic estimate has been made concerning nucleation time.

An alternate mechanism exists which could result in the formation of a suitable hole immediately after melting the sheet by Joule heating. This mechanism is suggested by Dombrowski and Fraser (27). They report that a particle with a diameter greater than the thickness of the sheet, will form a hole through the sheet if it is held in suspension and not wetted by the liquid sheet.

Therefore, any foreign particle in the gap region of the NiCr resistor, which has a diameter greater than 150 Angstroms and is not wetted by the molten NiCr, will form a hole through the molten sheet. This hole forms instantaneously upon melting.

It has been previously determined that a hole in a thin liquid sheet will be unstable and grow if its diameter exceeds the thickness of the sheet. Fraser (28) has derived an equation for the radial growth rate of such a hole. This equation is as follows:

$$\dot{e} = [2\gamma/h\rho_L]^{1/2}$$

Therefore, by inserting the proper values for NiCr, the following result is obtained:

$$\dot{e} = 178 \mu / \mu \text{ sec.}$$

From this it is obvious that if a suitable hole exists in the liquid NiCr sheet, it will grow and sever the sheet in much less than 1 microsecond.

If the sheet is at a uniform temperature, the hole will grow symmetrically in all directions. However, in the case of a NiCr resistor gap region, the temperature is not uniform. The gap region can be considered to be rectangular, with its long edge along the length of the resistor or perpendicular to the bus bar.

Initially, the hole in the sheet is circular with a diameter greater than the thickness of the sheet. The hole interrupts the continuity of the current flux lines and leads to current crowding between the edges of the circle and the near edges of the rectangular sheet. This current crowding leads to an increase in the Joule heating in these regions. The surface tension of the liquid NiCr is inversely proportional to the temperature. Therefore, the top and bottom regions of the hole, as seen in Figure 2, have lower than average temperatures and higher than average surface tensions. The opposite is true of the edges which have higher temperatures and lower surface tensions.

Therefore, if the expression for a spherical hole in equilibrium is examined (39),

$$\Delta P = 2\gamma/r$$

it is obvious that for small decreases in  $\gamma$ ,  $r$  must also decrease to preserve the equilibrium pressure difference. Thus, the hole will grow much faster towards the edges of the rectangular sheet where  $r$  is decreasing than towards the ends of the sheet where  $r$  is increasing. In short, the circle will degenerate into an ellipse and proceed to grow faster along its major axis than its minor axis as shown in Figure 2.

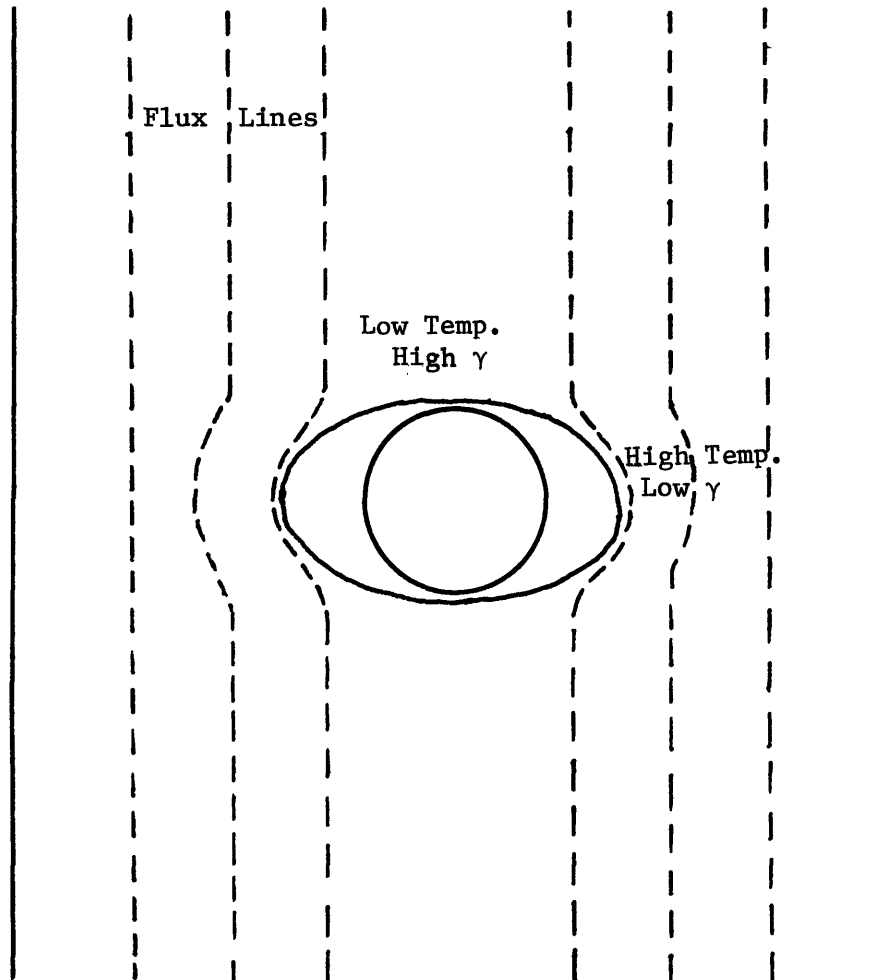


Figure 2: Illustration of current crowding and hole growth direction.



As the hole begins to grow out from its original shape, as described above, the edge of the film around the hole contracts and forms a cylinder. This cylinder is analogous to the Rayleigh jet (19) and as it thickens the characteristic perturbation develops on the rim. The amplitude of the perturbation grows until a drop forms on the surface of the rim. The diameter of the drop and the rim are approximately equal at this point. As the rim continues to contract the drop is left behind in the hole connected by a thread or finger.

If the central gap region remains molten while the hole continues to grow to the edge of the sheet, the fingers will also tend to pull back, form perturbations and separate into individual spherical particles. However, if the central gap region cools quickly as the hole and rim pull back, the drops at the tips of the fingers will freeze-in or solidify. However, the rim will still remain molten until the conductive path across the sheet is opened. Since it is still molten, it will continue to pull back leaving a series of long fingers extending into the gap region.

Therefore, two distinctly different structures can possibly exist in different gap regions. The particular structure developed will depend on the temperature of the gap region. This will depend on the extent of current crowding which is a function of resistor geometry.

In either case, the spacing between the fingers and the wavelength of the perturbation along the fingers should have the same value. Therefore, the spherical particles, which predominate in one case, should have

the same spacing as that observed between the long fingers in the other case.

The value of this spacing can be determined using Weber's (24) equation:

$$\lambda = 2\pi a [2(3Z+1)]^{1/2}$$

which is Rayleigh's equation, modified to account for viscosity. Using a range of viscosity values (1 to 5 centipoise), since no accurate value for NiCr could be obtained, the following range of values are obtained:

$$\lambda = 3040 \text{ \AA} \text{ for } \eta = .01 \text{ cp}$$

$$\lambda = 3580 \text{ \AA} \text{ for } \eta = .05 \text{ cp}$$

If Rayleigh's equation is used:

$$\lambda = 4.509(2a) = 2930 \text{ \AA}$$

The value of  $a = 325 \text{ \AA}$  is calculated from the average value of the spacing as given in Tables 1 and 2.

When the "bulk" of the sheet pulls back as the hole grows, a thin chromium oxide film is left in the gap region. This very thin oxide layer can also form holes and break-up. However, not enough is known about this grey film to make any definite statements. It will suffice to state that the grey oxide film does tend to break up into a honeycomb structure in the hotter gap regions whereas, only a few holes form between the tips of opposite fingers in the other gap regions.

An alternative approach to the fusing mechanism of NiCr resistors has also been developed. This approach also considers the gap region to be a thin liquid film.

It is proposed that a two-dimensional wave exists on the surface of the film. The waves should have a characteristic wavelength in both directions. The total surface area or total energy of the system is decreased as the amplitude of the waves increases. This is analogous to the effect of a perturbation growing on a cylindrical liquid rod as described by Lord Rayleigh (19).

When the amplitude of the waves exceed the half thickness of the film, a hole is formed, thus leading to the disintegration of the film. The amplitude of the two orthogonal waves need not be equal. However, if the amplitudes of these two waves are equal, a two-dimensional array of holes should form. These holes should pull back to form a honeycomb structure before finally coalescing to completely open the circuit.

If the amplitudes of the two waves are not equal, long holes should form in one direction corresponding to the wave with the larger amplitude. This could lead to a finger type structure after the holes have grown and the walls between them have broken up.

Examples of thin liquid sheets with these two-dimensional waves on their surfaces have been reported by Dombrowski and Fraser (27).

#### IV. Materials Preparation and Experimental Procedures


##### A. Introduction

The first step in this study of the fusing mechanism of NiCr resistors in PROM devices is to prepare acceptable samples for use in the transmission electron microscope. This entails preparing a thin section, which must be less than 2500 Angstroms in thickness and 3 millimeters in diameter, from a PROM device which is approximately 4 millimeters long, 2.5 millimeters wide and 7 millimeters thick. If this is accomplished, resolution on the order of 20 Angstroms can easily be obtained in the transmission electron microscope.

A sketch of the basic components of the PROM is given in Figure 3. Like any basic integrated circuit, it consists of a silicon single crystal base which is approximately 7 mils. thick. A thermal oxide layer of silicon dioxide, which is approximately 1 micron thick, is then grown over the silicon base. The next region consists of the metalization, that is, the aluminum bus-bars and emitter bases, the 150 Angstrom thick NiCr resistors, etc. Finally, a 1 micron thick passivation layer of silicon dioxide is evaporated over the metalization layer.

##### B. Sample Preparation

Both of the original techniques developed by Jones (1) and Devancy (17) demonstrate that the passivation layer can be successfully removed from an integrated circuit using a plasma etch. However, Devancy's (17) micrographs, taken on the scanning electron microscope, lack the resolution required for in depth studies of the fine structure of the gap



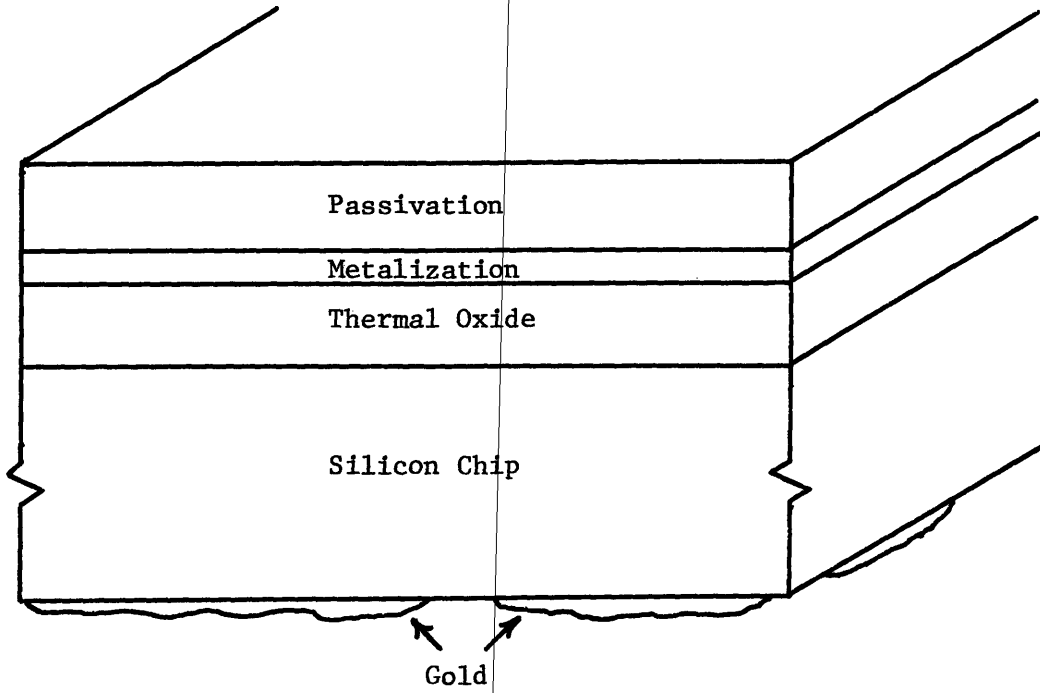


Figure 3: A sketch of the basic components of the PROM.

region. Also, these samples appear to be overetched, that is, all of the passivation has been removed and the NiCr resistors appear to have been slightly attacked by the plasma etch. Ideally, only 85 to 90 per cent of the passivation should be removed which leaves 1000 to 1500 Angstroms of silicon dioxide over the resistor. This guarantees that none of the gap components are lost to the plasma etch.

Jones (1), in going a step further, has successfully removed the silicon and silicon dioxide or thermal oxide layer from the back side of the device. Again, only 85 to 90 per cent of the thermal oxide should be removed. These specimens can then be examined in the transmission electron microscope which greatly improves the resolution in the gap region as recorded in the literature by Jones (1). However, these first thin-sections were rather thick which led to poor contrast in the micrographs.

Working with Jones, modifications have been made in his technique which resulted in the production of superior samples. As in the original process, carbontetrafluoride is the reactant gas used in the plasma etcher to remove 85 to 90 per cent of passivation layer. The sample is then mounted on a glass slide, back side up, and ground to partially remove the silicon base. After having polished the device to a final thickness of approximately 2 mils., the device is placed in the plasma etcher where the remaining layer of silicon and 85 to 90 per cent of the thermal oxide is removed. The resulting thin-section, which is approximately 2500 Angstroms thick, is then ready for examination in the transmission electron microscope. A complete description of this sample preparation technique is given in Appendix I.

## C. Observations and Measurements

### 1. Forward

Figure 1 is an illustration of the basic design of the NiCr resistors which make up the 2 dimensional matrix upon which the PROM device is based. The binary code of the computer is introduced by fusing these resistors in specific patterns. Since the NiCr resistor serves to close the circuit between the emitter based and bus bar, electrons can be drawn from the emitter base (which is connected to ground) and through the NiCr resistor by placing a positive potential on the bus bar. A resistor is fused by placing a sufficiently high positive potential on the bus bar to draw an excessive number of electrons through the NiCr resistor from the emitter base. The excessive pulse of current from the bus bar to the emitter base leads to Joule heating in the narrow region of the resistor where current crowding is most pronounced. This narrow region of the resistor then melts and pulls back to form a gap and open the circuit.

### 2. Transmission Electron Microscope Analysis

The Philips Em-300 transmission electron microscope is used to examine the gap region of the fused NiCr resistor. The EM-300 is operated at 100 kilovolts (KV) and all micrographs were taken in the bright field mode.

Figure 6 is a low magnification micrograph of the resistor matrix and serves to illustrate the arrangement of the bus bars, NiCr resistors and emitter bases.

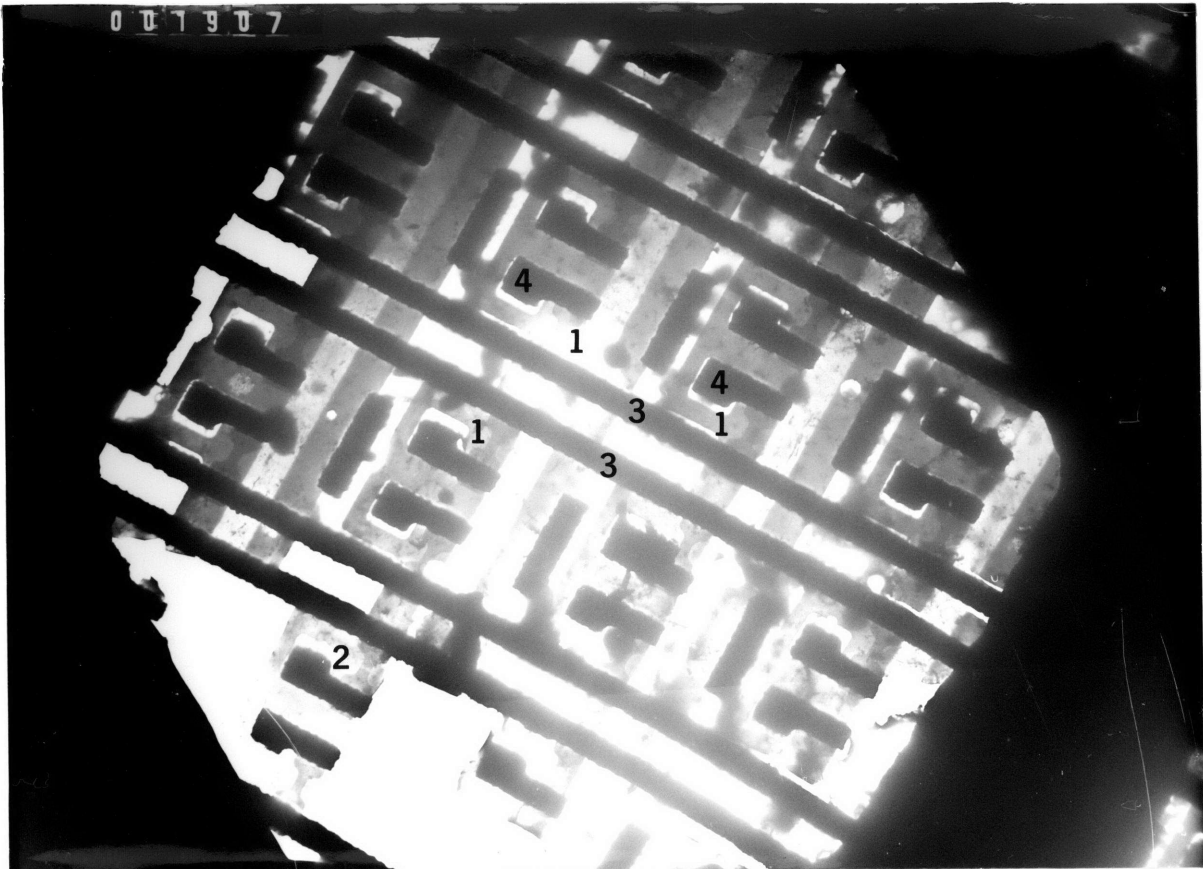


Figure 6: Low magnification micrograph of the resistor matrix, X450.

1. Unblown NiCr resistor
2. Blown NiCr resistor
3. Aluminum bus bar
4. Emitter base



NiCr resistors of two different geometric designs have been examined. Unblown resistors of these two designs are illustrated in Figure 7. Each design corresponds to the type of NiCr resistor manufactured by two independent vendors. These designs will be referred to in future discussions, as Type A and Type B as labelled in Figure 7.

As previously stated, the PROM device is programmed by fusing the NiCr resistors in specific patterns. When the resistor is fused a molten zone is formed in the narrow region of the resistor which pulls back to form a gap and open the circuit. It is interesting to note that there is a heat-effected zone associated with the molten zone. This is illustrated in Figure 8 where the elongated grains (due to directional grain growth) define this heat-effected zone. However, this zone is not observed as a general feature of fused resistors and has only been recorded on this one micrograph.

The fine features of the structure found in the gap region of the Type A NiCr resistors is well illustrated in Figures 9 through 12. There are certain features of the structure of the gap region that are characteristic of Type A resistors. These features are listed below.

a) After the molten zone formed, 2 interfaces appear to have developed, separating the resistor into two sections. These interfaces then appear to have "pulled back" forming an unstable meniscus. This unstable meniscus is characterized by the long fingers or rods of NiCr which extend into the gap region.

b) The fingers are characteristically arranged at specific intervals across the width of the resistor.

c) The fingers also seem to have partially pulled back leaving elliptical and spherical particles between themselves and their sister fingers across the gap.

d) White holes are usually found in the region between the ends of the fingers. These white spots are referred to as holes because they represent areas of high electron transmission which suggests that all of the nichrome has been removed from these areas.

e) Except for the white holes, a continuous light grey phase remains to outline the original position of the unblown resistor.

f) The fingers on the emitter base side of the gap are much longer and wider than those on the bus bar side of the gap. However, the fingers on opposite sides of the gap are usually arranged in brother-sister pairs.

The structure found in the gap region of the B Type NiCr resistors, as illustrated by Figures 13 through 15, appears to be very different from that found in the A Type gap regions. Certain features of the structure of the gap region are characteristic of B Type resistors and are listed below.

a) Dense spherical particles are distributed throughout a major portion of the gap region. These particles are arranged with a specific spacing, that is, there tends to be common nearest neighbor spacing.

b) The spherical particles are always surrounded by an interconnected grey phase.

c) Although all of the spherical particles are interconnected by the grey phase, they are also all separated by white holes. As discussed before, these white holes are areas of high electron transmission.

This honeycomb structure is common to all B Type resistor gap regions and appears to be completely unrelated to the finger structure found in A Type resistor gap regions. This point shall be considered later.

One of the most outstanding features of the A Type resistor gap region is the periodic spacing of the NiCr fingers. The average value of the "true spacing" of the fingers, as defined by Underwood (18), is given in Table I. These true spacing values were measured from Figures 9 and 11.

It is also observed that the NiCr fingers of the Type A gap region have partially pulled back. In doing so, perturbations with specific wavelengths have developed on the surface of the fingers or rods of NiCr. In several instances these perturbations have led to the break-up of the fingers. This results in the formation of elliptical and spherical particles which are arranged at periodic intervals away from the tip of the finger. The wavelength of the perturbation on the finger equals the spacing between the resulting particles. This wavelength is also recorded in Table I as measured from Figures 9 and 11. It should be noted that the wavelength of the perturbation and equivalent spacing between the resulting particles is approximately equal to the spacing between the fingers.

As previously stated, the spherical particles found in the gap region of the B Type resistors are arranged with a specific spacing. The average value of this spacing has been measured from Figures 13 and 15 and is recorded in Table II. A comparison of the values listed in Tables I and II demonstrates that the spacing between the particles in the B Type gap region is approximately equal to the spacing between the fingers in the A Type gap region. This point will be examined in more detail in future discussions as it is the link that joins the Type A and B resistors together under one fusing mechanism.

### 3. Scanning Transmission Electron Microscope Analysis

An attempt has been made to determine the chemical composition of the different components found in the Type A gap regions. A JEOL 100-C scanning transmission electron microscope (STEM) was used because, with this instrument operating in STEM mode, X-ray data can be collected from spots having diameters of approximately 500 Angstroms. This small spot size is essential since most of the components of the gap region have dimensions in this range. A Cambridge scanning electron microscope was also used, in STEM mode, in an attempt to continue the initial work using the JEOL 100-C. Unfortunately, insufficient data has been collected to establish any general conclusions regarding the chemical composition of the gap components. However, the data collected does suggest that some mode of segregation is taking place with different gap components having very different compositions.

#### 4. Analysis of Micro-micro Electron Diffraction Patterns

The atomic structure of the components of the A Type gap region has also been investigated. Both the Philips EM-300 and the JEOL 100-C have proven to be ineffective in producing useful electron diffraction patterns of the gap region. However, the JEOL 200-C, with its 200 kilovolt electron source, can produce micro-micro diffraction patterns of the components in the gap region. Also, a spot size of approximately 500 Angstroms can be used to generate the micro-micro diffraction pattern. Therefore, patterns can be obtained from individual components within the gap region. Unfortunately, during the initial study conducted at the University of Illinois, the JEOL 200-C could not be operated at 100 per cent efficiency. Under these less than optimum conditions, exposure times for the micro-micro diffraction patterns were approximately 7 minutes. The pattern then had to be displaced in the field of view in order to photograph the outer rings. The sequence of micro-micro diffraction patterns taken for one spot in the grey phase of a Type A gap region is given in Figure 16. This pattern has been indexed as a combination of chromium oxide ( $\text{Cr}_3\text{O}_4$ ) and an impure silicon oxide phase.

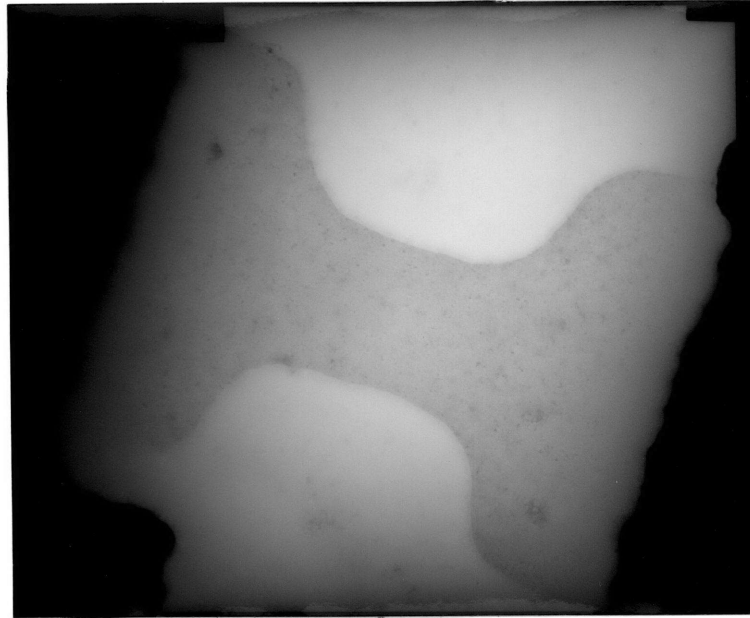
From Figure 16, it is observed that the patterns are elliptical. In order to index these patterns, the camera constant had to be calculated for the major and minor axis of the elliptical pattern produced by a known standard. The pattern for the standard had to be generated using exactly the same operating conditions as was used to produce the micro-micro diffraction patterns of the gap components.

Unfortunately, insufficient data was obtained from this initial study. Therefore, the atomic structures of specific components in the gap region

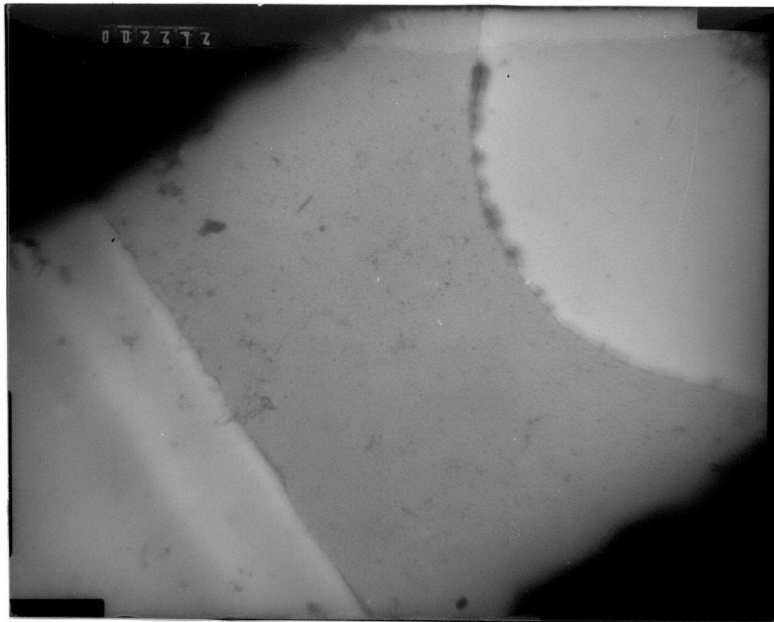
have not been identified. However, the identity of several phases present in this region has been obtained. The three phases present are:

- 1)  $\text{Cr}_3\text{O}_4$
- 2) impure silicon oxide
- 3) NiCr (80:20)

The NiCr phase was indexed from micro-micro diffraction patterns taken in the region adjacent to the bus bar, away from the gap area. The impure silicon oxide and NiCr phases were indexed from patterns obtained from the grey phase found in the gap region.



a) Type A, x6,300



b) Type B, x10,400

Figure 7: Unblown resistors of: a) Type A,  
b) Type B.

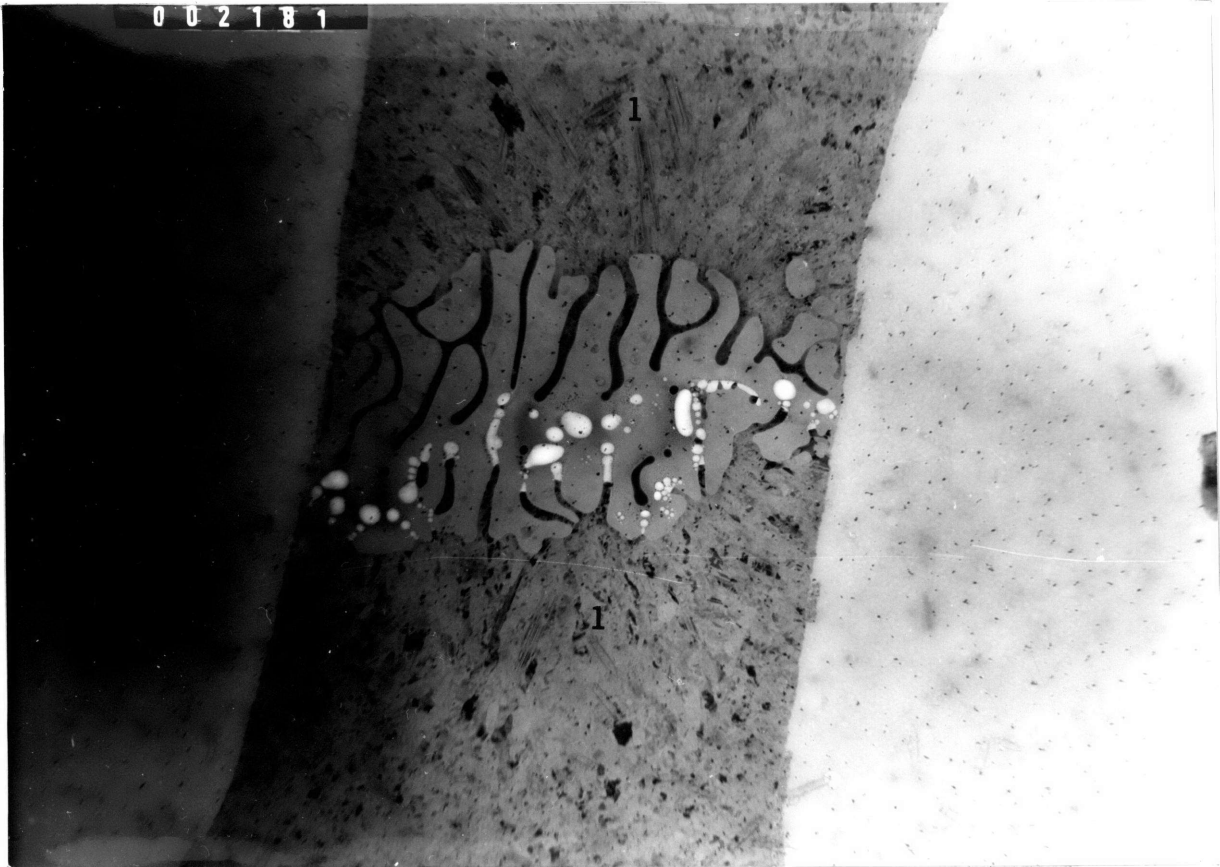


Figure 8: Illustration of the heat-effected zone associated with the molten zone or gap region of the Type A resistor, X21,000.

1. Heat-effected zone



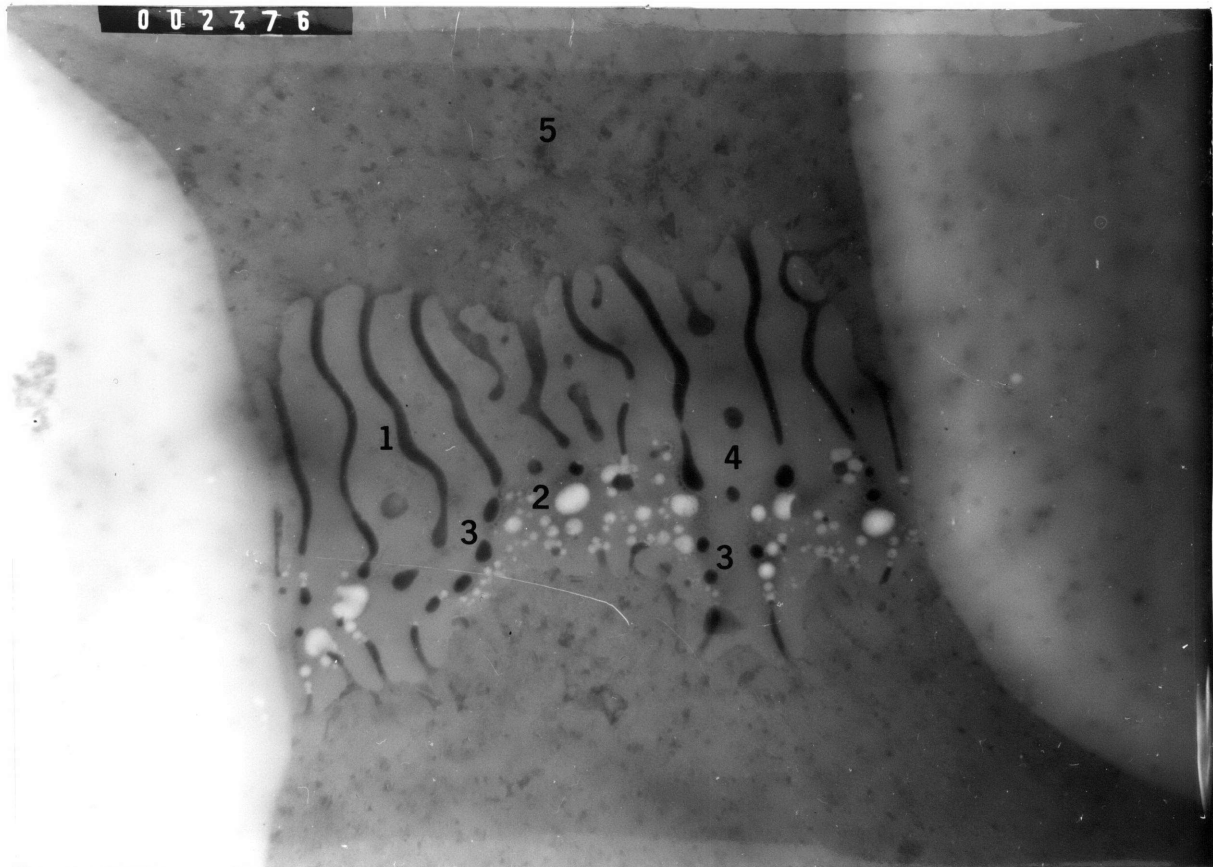


Figure 9: Gap region of fused, Type A resistor, X26,000.

1. Fingers
2. Holes
3. Elliptical and spherical particles
4. Grey phase
5. Emitter base side of gap region

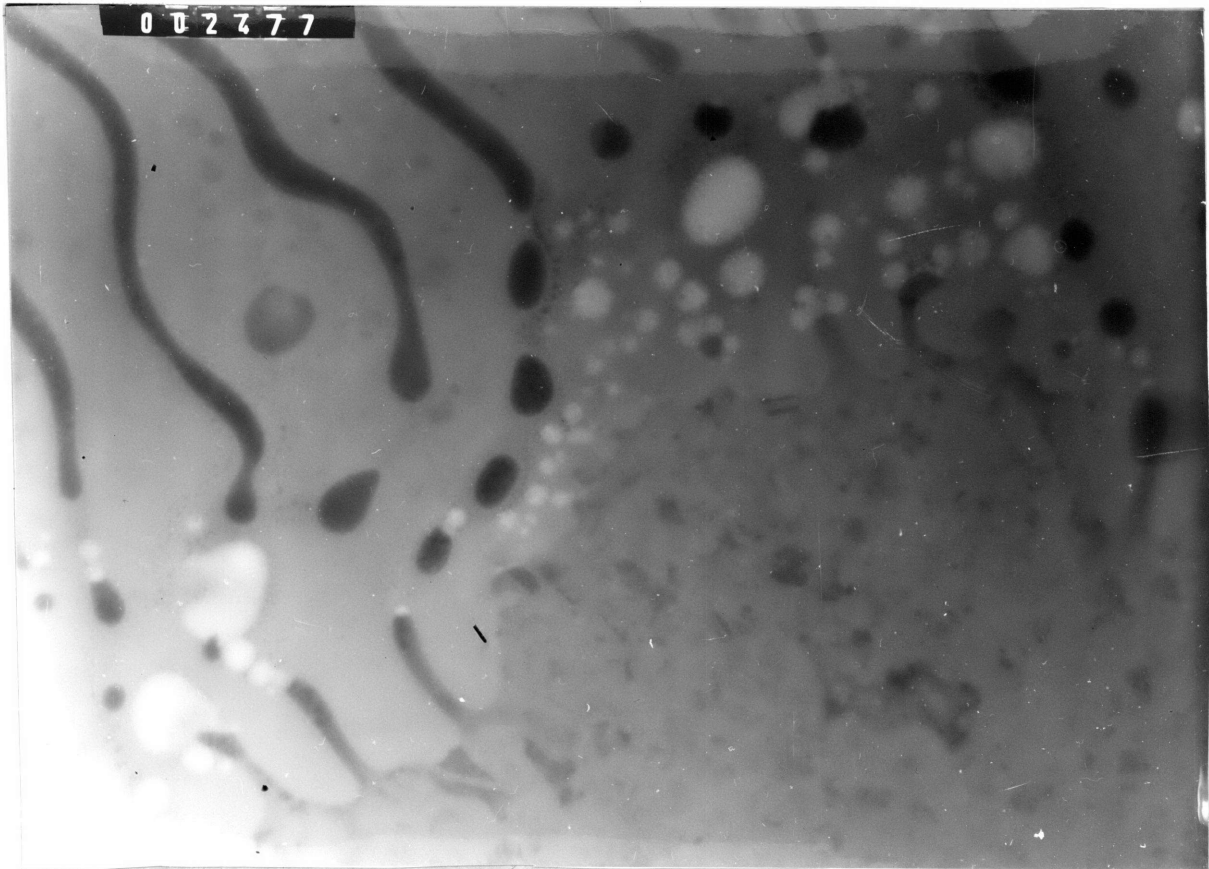


Figure 10: Higher magnification of Figure 9, X66,000.

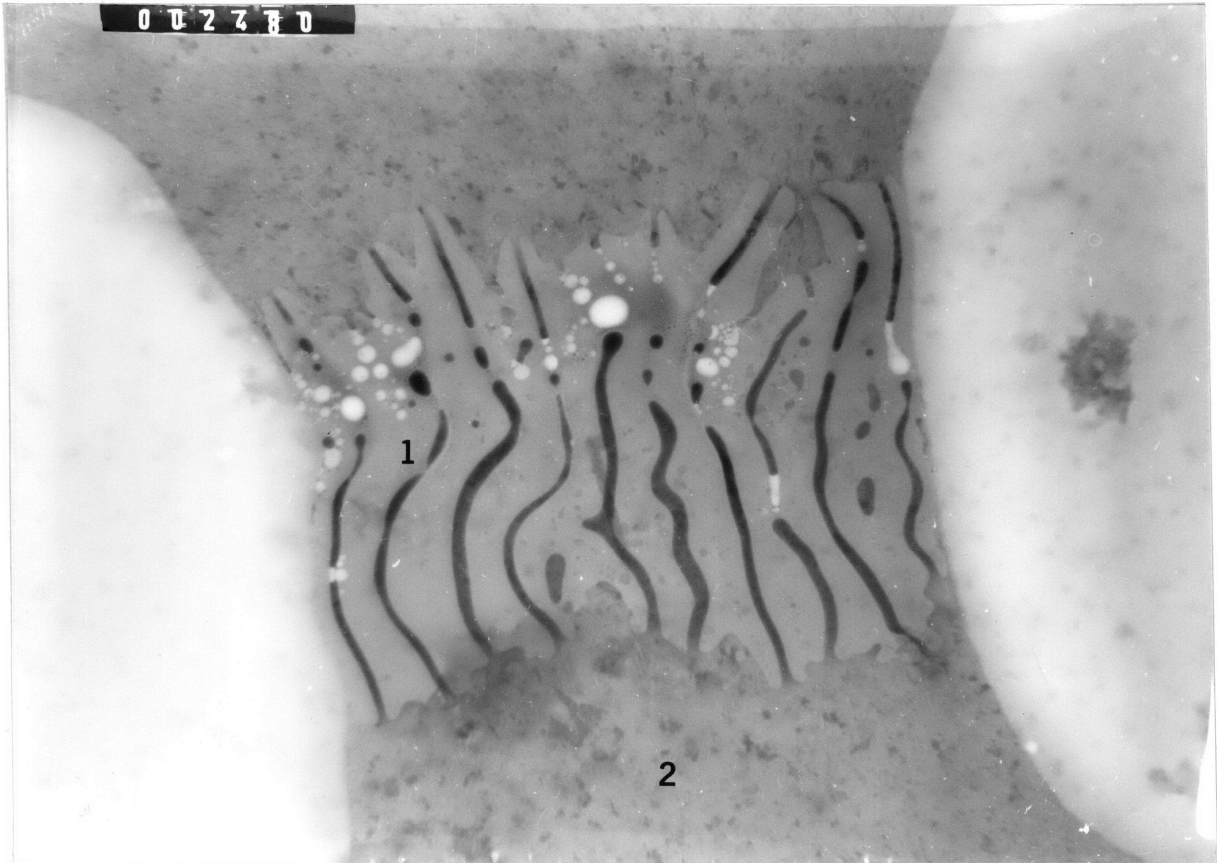


Figure 11: Gap region of fused, Type A resistor,  
X26,000.

1. Perturbation with characteristic wavelength along NiCr finger.
2. Emitter base side of gap region

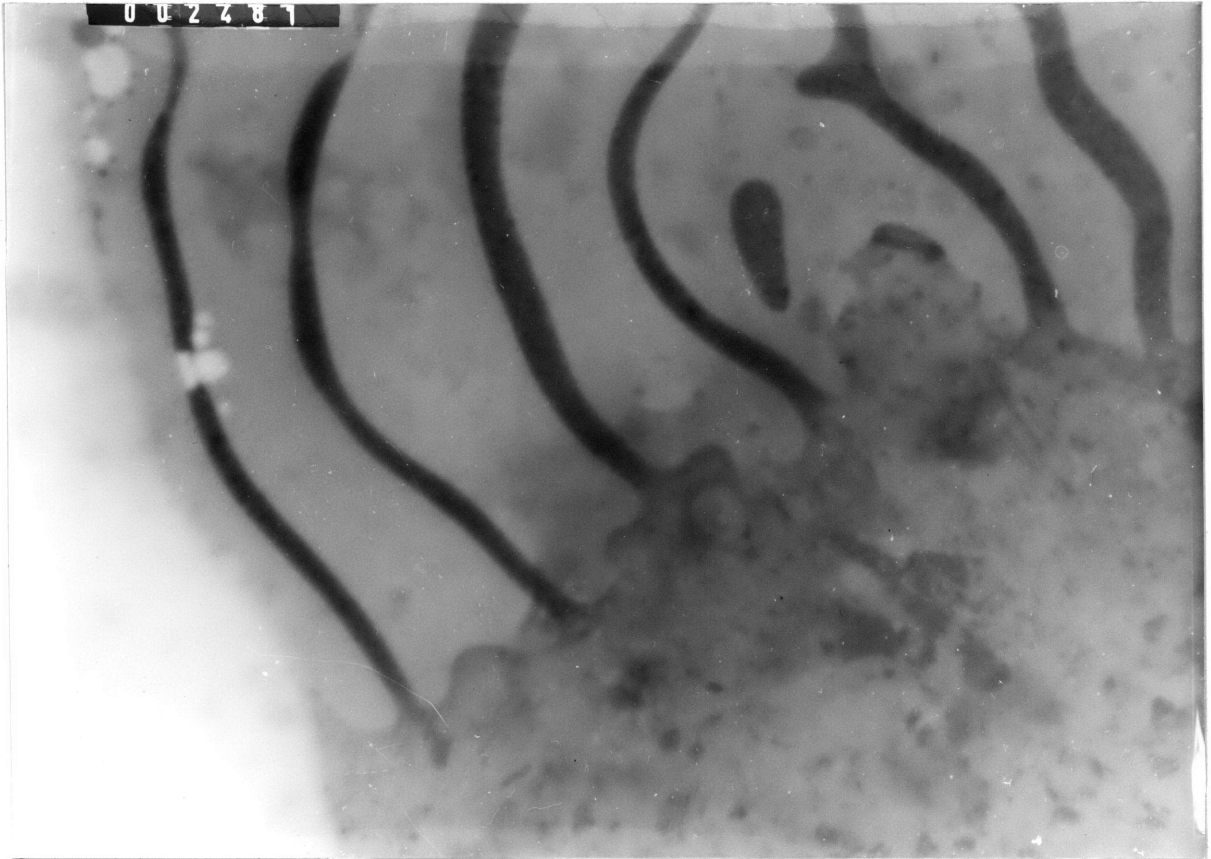


Figure 12: Higher magnification of Figure 11. Illustrates periodic spacing between the fingers, X66,000.



Figure 13: Gap region of fused, Type B resistor, X21,000.

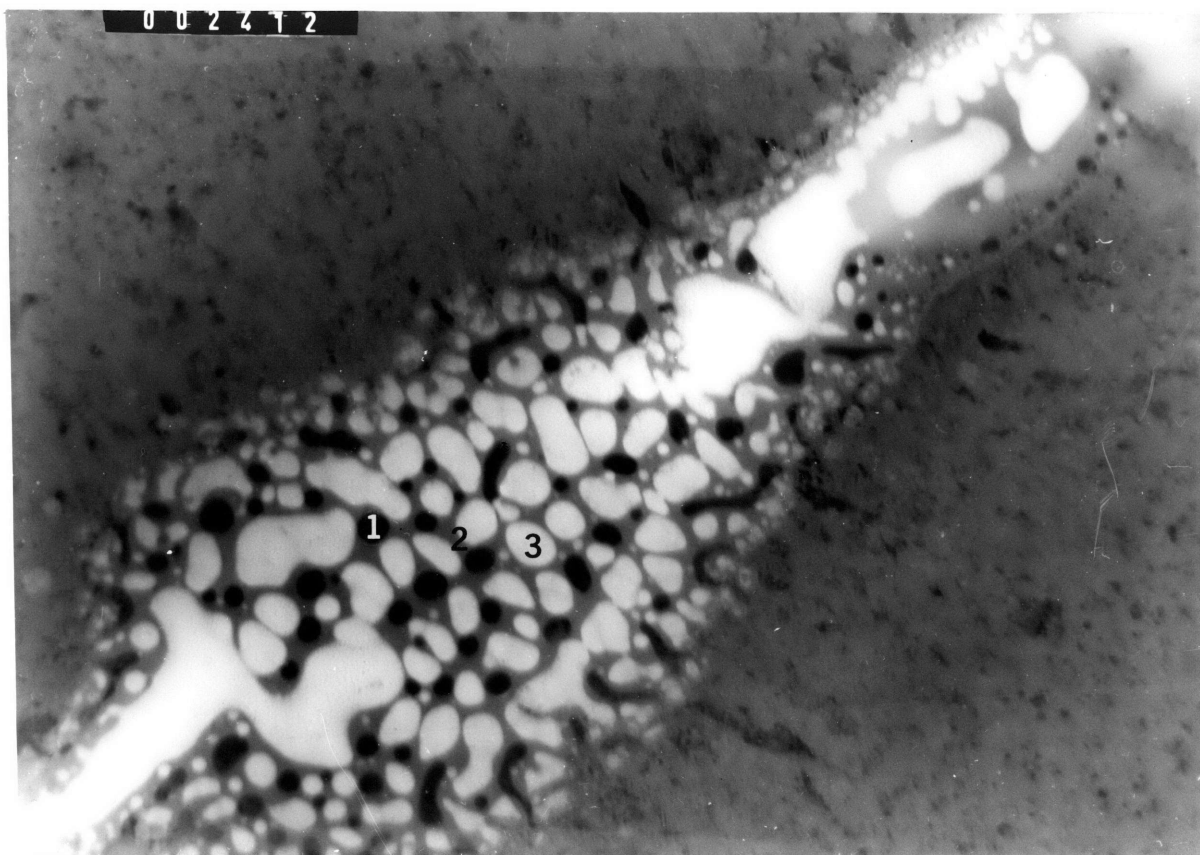


Figure 14: Higher magnification of Figure 13, X43,000.

1. Spherical particles
2. Interconnecting grey phase
3. White holes

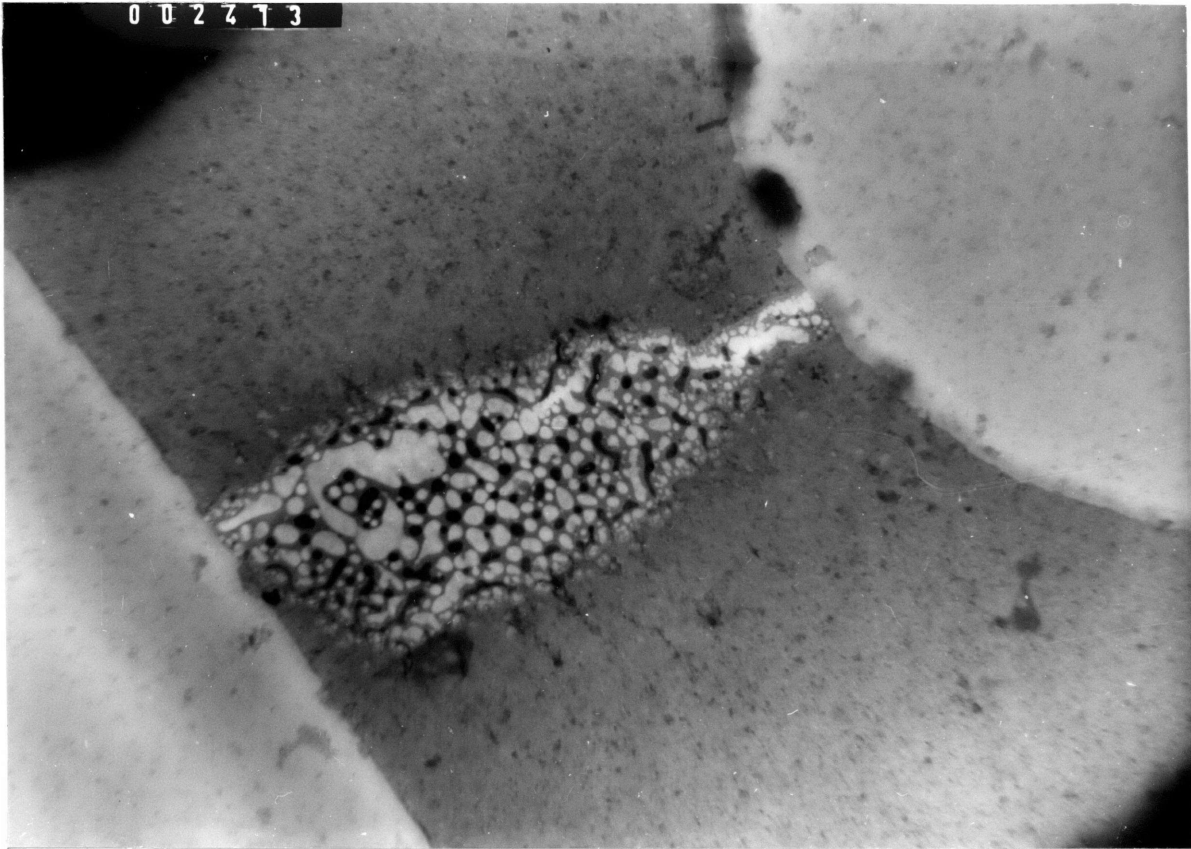


Figure 15: Gap region of another fused, Type B resistor,  
X21,000.

Table I						
Figure	9	S. Dev.	Var.	11	S. Dev.	Var.
$\lambda' (\text{\AA})$	2409	.206	.039	2286	.235	.051
$\lambda (\text{\AA})$	2269	.256	.057	2171	.141	.018

Table I: Measured values of:  $\lambda'$  = spacing between fingers

$\lambda$  = wavelength of perturbation along surface of finger

Calculated values of:

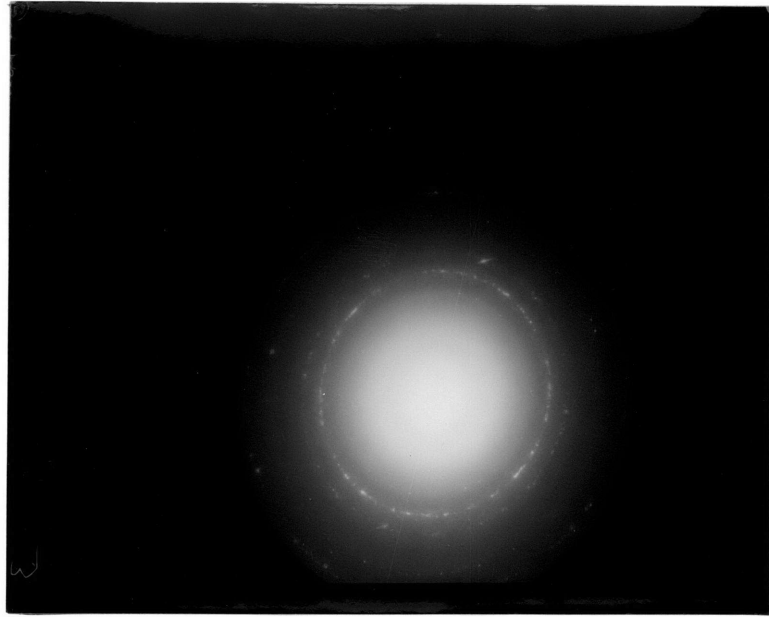
$$\text{Standard Deviation (S. Dev.)} = \left[ \frac{\sum_{n=1}^N (x_n - \bar{x})^2}{(N-1)} \right]^{1/2}$$

$$\text{Variance (Var.)} = \frac{\sum_{n=1}^N (x_n - \bar{x})^2}{N}$$

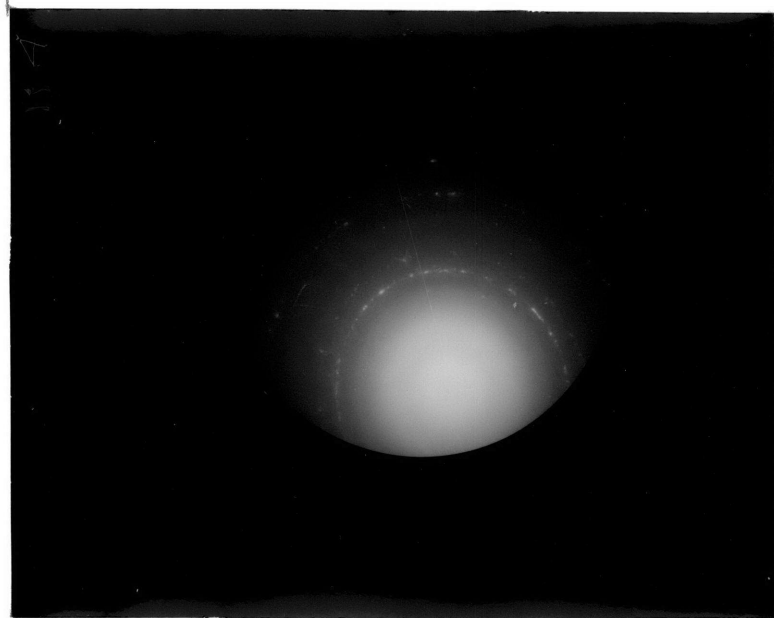
Table II			
Figure	$\delta$	S. Dev.	Var.
13	2338	.113	.012
15	1953	.087	.007

Table II: Measured values of:  $\delta$  = the spacing between the spherical particles





a) Centered



b) Displaced

Figure 16: Micro-micro diffraction patterns of grey phase in Type A gap region.

## V. Discussion of Results

The theoretical treatment of the fusing mechanism of NiCr resistors in PROM devices, as presented here, is discussed from the initial current pulse to the final freezing-in or solidification of the gap region. All observations and measurements of the gap region were made either before or after the resistor had been fused. Therefore, only the final structure of the gap region, as predicted by the theory, can be compared with the micrographs of the gap region.

The type A resistor gap region is characterized by an arrangement of long fingers. This structure has been predicted to exist for a resistor whose central open region solidifies before the circuit has completely opened. This phenomenon would usually be associated with resistors having large gap regions where large temperature gradients could exist. The resistor is melted by Joule heating in regions where current crowding occurs, that is, around the rim of the expanding hole. However, Joule heating does not occur along the length of the finger. The finger is therefore, quickly cooled by the surrounding glass phase. Thus, the tip of the finger could possibly solidify while the rim of the hole is still contracting, therefore, producing elongated fingers. This does not mean that the fingers do not contract. They do, however, this motion is controlled by the temperature in the gap region.

The spacing between the fingers and the wavelength of the perturbation along the fingers can be calculated using the equations of Rayleigh (19) and Weber (24). The Rayleigh equation, based only on

surface tension, predicts a value of approximately  $2000 \text{ \AA}$  which is in excellent agreement with the measured values given in Table I. Weber's equation, which accounts for viscosity effects, predicts a value of approximately  $3000 - 3600 \text{ \AA}$  which is also in good agreement with the measured values from Type A resistors.

The theoretical analysis was based on the assumption that a thin sheet existed in a homogeneous phase. Therefore, the existence of the grey phase and the subsequent white holes could not be predicted to exist. The observation can be made that the white holes do exist between the ends of opposite fingers which corresponds to the hottest region of the gap as the hole grows. Therefore, it can be assumed that the grey phase ( $\text{Cr}_3\text{O}_4$ ) will break up when the temperature is sufficiently high.

It is observed that the fingers are longer on the emitter base side of the gap of a fused Type A resistor. This could be due to the effect of the force of the electric field in the resistor which acts in the direction opposite to electron flow. Therefore, the electric field assists surface tension in pulling the rim of the hole back in the direction of the emitter base. It would simultaneously retard the motion of the opposite side of the hole in the opposite direction.

The phenomenon of brother-sister pairs of fingers is due to the existence of identical waves on the opposite sides of the hole or gap. Since these waves will obviously have the same wavelength, they will have the same nodal points since they are both terminated at the same point

on the edges of the hole or gap. Thus, corresponding nodal points define the position of corresponding brother-sister pairs.

The Type B resistor gap regions are characterized by an arrangement of spherical particles. This structure has been predicted for a completely molten sheet. In this case, the hole forms and grows, leading to the production of fingers which also contract and break up. Therefore, the spacing measured between the particles should correspond to the value predicted by Rayleigh (19) and Weber (24). Again, as with the Type A resistor, the measured (Table II) and calculated values are in very good agreement.

The gap region of the Type B resistors is hot enough for all of the fingers to disintegrate. Therefore, the grey phase might be expected to break up since the region appears to be hotter. This is indeed what is observed and the characteristic honeycomb structure results.

Therefore, the dissimilar Type A and Type B gap region structures are not formed by different fusing mechanisms but by a variation in one general mechanism which is apparently due to the temperature and size variation of the gap region produced. Therefore, resistors of a different design could possibly produce gap regions with a structure exhibiting features of both of the A and B Type gap regions.

## VI. Summary and Conclusions

The NiCr resistors used in PROM devices are fused or blown by pulsing an excessive amount of current through it. This leads to Joule heating in the narrow region of the resistor where the current crowding is most pronounced. The resistor then melts and pulls back to open the circuit and thus introduce the binary code to be used.

From the theoretical treatment, observations and measurements, it is concluded:

1. The formation of a hole prior to or immediately after melting, is essential to the fusing mechanism. This hole could be produced by an electromigration process, an unwetted, suspended particle or a surface wave with an amplitude greater than half the thickness of the molten sheet.
2. The hole grows into a flattened ellipse due to the asymmetric surface tension.
3. As the hole grows, its rim thickness into an unstable cylinder which then disintegrates into a symmetrical system of fingers extending into the hole.
4. The fingers will or will not disintegrate into elliptical and spherical particles depending upon the temperature and size of the gap region.
5. One fusing mechanism, based on jet and sheet instability as illustrated by Rayleigh (19) and Dombrowski (27), is operative.
6. By changing the fusing conditions, the final structure of the gap region will appear to be quite different. However, this is due only

to changes in the extent of the fusing process and not to a change in fusing mechanism itself.

7. The sum total of all steps in the theoretical process can occur in less than 1 micro-second.

## VII Suggestions for Future Work

The theoretical fusing mechanism of NiCr resistors, as presented here, answers several questions while posing and leaving many more unanswered. The following suggestions for future work should yield the solutions to many of these questions and further qualify the fusing mechanism.

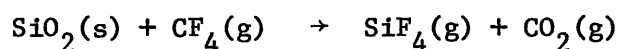
1. Determine the current density which initiates electromigration. Pulse a series of resistors at successively higher levels until a resistor blows. Examine these series of resistors in the transmission electron microscope at high magnifications to determine the presence or absence of voids due to electromigration.
2. Investigate the possible existence of impurities in the NiCr resistor which, upon melting, result in unwetted particles and subsequently holes.
3. Establish a technique for either:
  - a. Photographing the fusing mechanism while in progress.
  - b. Halting the fusing process before it can run to completion.
4. Complete the micro-micro diffraction analysis to identify the components of the gap region.
5. Complete the scanning transmission electron microscope analysis to determine the extent of the elemental segregation.

## APPENDIX I

## SAMPLE PREPARATION

The plasma etcher is used because it offers a controlled method for uniformly removing thin films of silicon and silicon dioxide. A Plasmod Plasma Etcher, manufactured by the Tegal Corporation, is used. The complete etching apparatus consists of a gas supply, the Plasmod with its radio frequency (RF)-generated-plasma reaction chamber and a mechanical vacuum pump as sketched in Figure 4.

When a reactant gas, in this case carbon tetrafluoride, is fed into the reaction chamber of the Plasmod, which is maintained at approximately 1 torr, a low-temperature plasma is produced by the RF generator. This plasma or ionized gas then converts the solid species, with which it is reactive, into a gaseous phase. The reaction for the case of silica removal, as reported by Jones (1), is:



One advantage of this process is that the reaction proceeds at approximately 100° Centigrade (C).

The PROM device is removed from its ceramic package by heating the device on a hot plate to melt the gold bond between the two. This leaves a gold residue on the base of the PROM device as depicted in Figure 3. This gold residue must be removed to avoid the formation of gold fluorides in the plasma etcher. This unstable gold phase will redeposit on the surface being etched and act to retard the etching process locally, thus



leading to non-uniform etching conditions.

The PROM device is mounted on a glass slide, bottom side up, using a thermoplastic cement (Canada Balsam) and the gold is then polished away using 600 grit Alumina paper. The device is then removed from the glass slide and ultrasonically cleaned in acetone to remove all thermoplastic residues.

The sample, being 4 millimeters long and 2.5 millimeters wide, must now be diced because the maximum diameter of samples that can be used in the transmission electron microscope is 3 millimeters.

The diced sections are then placed, passivation side up, on a glass slide and introduced into the plasma etcher where 85 to 90 per cent of the passivation is removed. Monitoring the removal rate or measuring the final thickness of the passivation layer is very difficult. This is usually accomplished by monitoring the undercutting and changes in color optically or by monitoring changes in resolution in the gap region using the scanning electron microscope.

The sample is again mounted on a glass slide with its bottom side up as in Figure 5a. The sample is then gently polished by hand using 600 grit Alumina paper until it begins to crack and break up around the edges. The polishing is then continued on 4/0 emery paper with oil until the sample again begins to break up around the edges. The sample has now been reduced to approximately 2 mils. in thickness. The sample is now removed from the glass slide and again ultrasonically cleaned.

The remaining thickness of silicon and 85 to 90 per cent of the thermal oxide layer must now be removed using the plasma etcher.

However, the passivation surface and sides of the sample must be protected from further etching. This is done by placing the specimen on a drop of diffusion pump oil which acts as a protective coating. The oil polymerizes after being subjected to the plasma etch for only a minute. Thus, it also acts as a cement and holds the specimen in place on the glass slide. After the silicon has been removed the sample becomes transparent. The thickness of the thermal oxide can then be monitored by noting the color sequence that the NiCr resistors go through as the thermal oxide thickness decreases. Therefore, when the NiCr resistors become a specific color, light brown or tan, the thermal oxide appears to be approximately 1500 Angstroms thick.

The sample has now been sufficiently thinned and the NiCr resistors should be sandwiched between the 1000 to 1500 Angstrom thick layers of thermal oxide and passivation as depicted in Figure 5b. These two layers of glass guarantee that no modifications have been made in the fine structure found in the gap region of the fused resistor.

The finished sample can be successfully removed from the glass slide by submerging the slide in a beaker of acetone. The polymerized oil is soluble in acetone and the specimen will soon be floating freely. The sample can now be dipped from the beaker using a standard folding grid. Extreme caution must now be exercised because the sample tends to curl into a cylindrical shape. If necessary, it must be held flat with a pair of tweezers while the grid is folded and locked over it. This completes the process and the sample is ready for observation in either the scanning or transmission electron microscope.

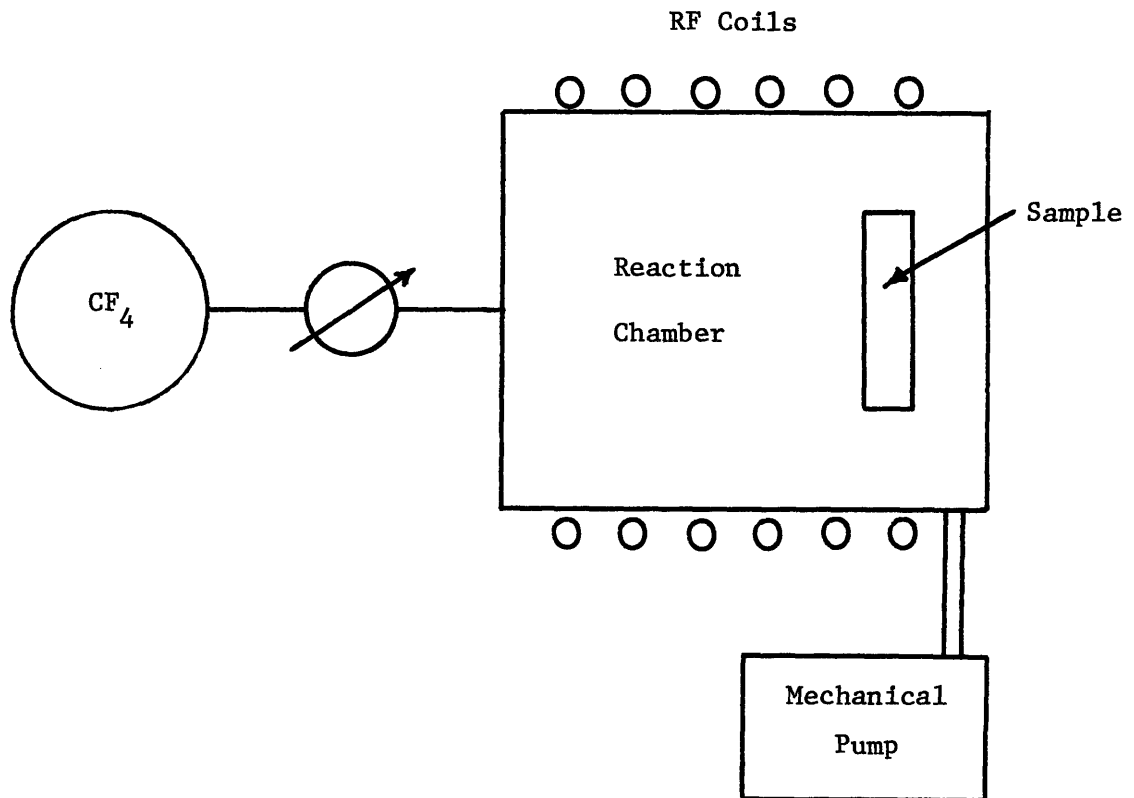


Figure 4: A schematic of the complete plasma etching apparatus.

1. RF - generated-plasma reaction chamber.
2. Carbon tetrachloride ( $CF_4$ ) gas supply and control section.
3. Vacuum system.

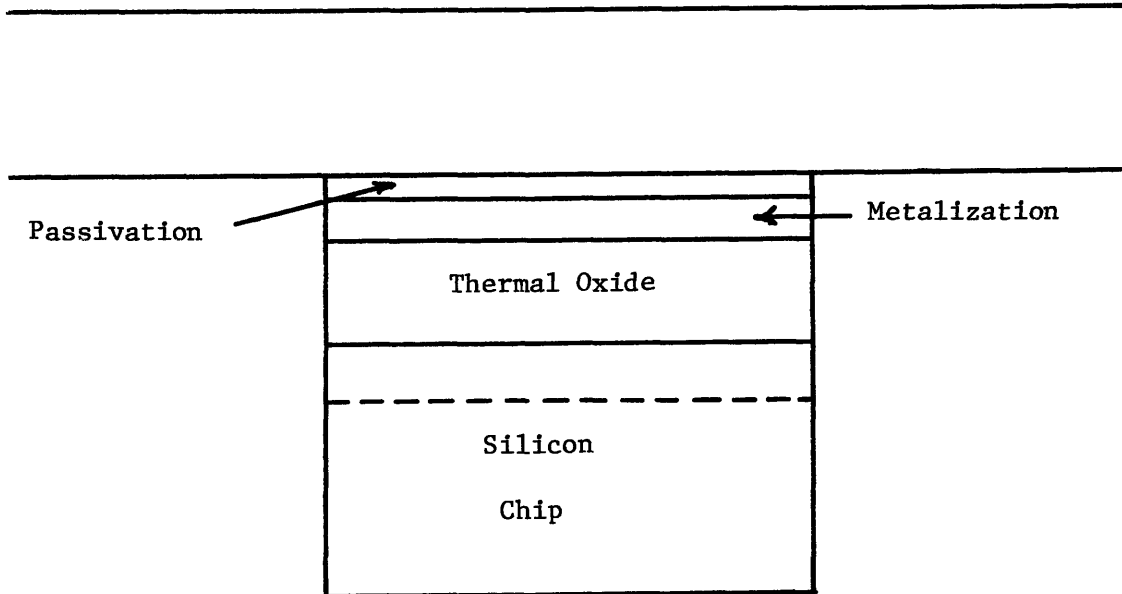


Figure 5,a. Illustration of the position of the sample prior to mechanical polishing to partially remove the silicon.

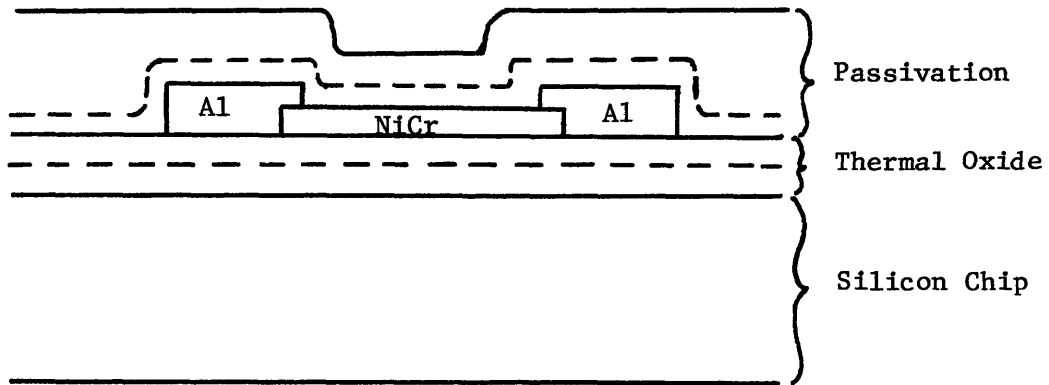


Figure 5,b. Schematic illustration of the initial and final thickness of the sample, where the dotted lines outline the final thickness.

## APPENDIX II

## SYMBOLS

Roman

a	Radius (variable)
A	Coefficient
d	Diameter
e	Exponential
$\dot{e}$	Radial velocity of hole
G	$= 4\gamma/h\rho_L$
$\Delta G$	Free energy change
h	Thickness of the sheet
$J_0$	Bessel function of zero order
k	$= 2\pi/\lambda$
K	Curvature
$\Delta P$	Pressure inside minus pressure outside
q	Rate of growth of disturbance
r	Radius
$r^*$	Critical radius
R	Reynold's number
S	Vacancy supersaturation
t	Time
T	Kinetic energy
U	Velocity
V	Potential energy
W	Weber number

Roman

$z$  Axis of cylinder

$Z = W/R$

Greek

$\alpha$  Variable amplitude of perturbation

$\gamma$  Surface tension

$\gamma_b$  Grain boundary energy

$\gamma_S$  Surface energy of void-metal interface

$\delta$  True spacing of particles in Type B gap regions

$\Delta$  Difference

$\eta$  Viscosity

$\lambda$  Wavelength of perturbation along cylinders of NiCr

$\lambda'$  Wavelength between fingers in Type A gap region

$\mu$  Micro

$\Delta\mu$  Energy gained per vacancy

$\rho$  Density

$\rho_L$  Density of liquid

$\sigma$  Surface area

$\phi$  Velocity potential

$\Omega$  Atomic volume

$\infty$  Infinity

Subscripts

b Grain boundary

S Surface

L Liquid

Variables	NiCr	Reference
$\gamma_s \left(\frac{\text{ergs}}{\text{cm}^2}\right)$	30	37
S	0.1	34
$\gamma \left(\frac{\text{dynes}}{\text{cm}}\right)$	$\sim 1700$	38
h (Å)	150	1
$\rho_L \left(\frac{\text{gm}}{\text{cm}^3}\right)$	$\sim 7.1$	38
a (Å)	325	+
$\eta$ (cp)	.01-.05	40
$\gamma_s \left(\frac{\text{ergs}}{\text{cm}}\right)$	30	37
S	.1	34

Table III: Values of variables used.

+ Measured

## IX Bibliography

1. W. K. James; 12th Annual Proc. Reliability Phys. Symp., IEEE, Las Vegas (1974).
2. L. I. Maissel, R. Glang; "Handbook of Thin Film Technology," McGraw-Hill Book Company (1970).
3. R. W. Berry, P. M. Hall, M. T. Harris; "Thin Film Technology," D. Van Nostrand Company (1968).
4. K. L. Chopra; "Thin Film Phenomena," McGraw-Hill (1969)
5. R. W. Bicknell, H. Blackburn, D. S. Campbell and D. J. Stirland; Microelectronics and Reliability, Vol. 3 (1964), p. 61-64.
6. A. Taylor, K. G. Hinton; J. of the Inst. of Metals, Vol. 81 (1953), 169-180.
7. A. Taylor, R. W. Floyd; J. of the Inst. of Metals, Vol. 80 (1952), p. 577-587.
8. E. Philofsky, G. Stickney, K. V. Ravi; 8th Annual Reliability Phys. Conf., IEEE, Las Vegas (1970), p. 191-199.
9. M. Hansen; "Constitution of Binary Alloys," McGraw-Hill (1958).
10. T. K. Labshmanan; Trans. of 8th National Vacuum Symp., Vol. II (1962), p. 868-873.
11. J. Ahern, K. Heid; presented at Inter. Microelectronics Sym. (1970), p. 10-13.
12. C. W. Lewis, J. J. Bohrer; "Physics of Failure in Electronics," Spartan Books, Inc. (1963), p. 11-19.
13. M. Goldberg, A. Horberg, R. Stewart and D. Levinson; "Comprehensive Failure Mechanism Theory-Metal Film Resistor Behavior," Phys. of Failure in Electronics, Vol. II (1963), p. 68.
14. M. Nagata, K. Utino, A. Aritomo, and M. Oishi; Electronic Components Conf. (1969), p. 359-366.



15. W. F. Keenan, W. R. Runyan; *Microelectronics and Reliability*, Vol. 12 (1973), p. 125-138.
16. R. S. Mo, D. M. Gilbert; *J. of the Electrochemical Soc.*, Vol. 120, No. 7 (1973), p. 1001-1003.
17. J. R. Devaney, A. M. Sheble III; *12th Annual Proc. Reliability Phys., Sym.* (1973).
18. E. E. Underwood; "Quantitative Stereology," Addison-Wesley (1970), p. 74.
19. Lord Rayleigh; *Proc. Lond. Math. Soc.*, Vol. 10 (.879), p. 4-13.
20. Lord Rayleigh; *Phil. Mag.*, Vol. 34 (1892), p. 177-180.
21. Lord Rayleigh; *Phil. Mag.*, Vol. 48 (1899), p. 321-337.
22. Sir H. Lamb; "Hydrodynamics," Dover Publications (1945), Article 274.
23. Lord Rayleigh; *Phil. Mag.*, Vol. 34 (1892), p. 145-154.
24. C. Weber; *Z. angew. Math. Mech.*, II (1931), p. 136.
25. C. C. Miesse; *Ind. and Eng. Chem.*, Vol. 47, No. 9 (1955), p. 1690-1701.
26. R. S. Brodkey; "The Phenomena of Fluid Motions," Addison-Wesley (1967), Chap. 17.
27. N. Dombrowski, R. P. Fraser; *Phil. Trans. Roy. Soc. Lond.*, Series A., Vol. 247 (1955), p. 101-130.
28. R. P. Fraser, P. Eisenklam, N. Dombrowski, D. Hasson, *J. A. I. Ch. E.*, Vol. 8, No. 5 (1962) p. 672-680.
29. J. R. Black; *IEEE Trans. on Electron. Devices*, Vol. ED-16, No.4 (1969), p. 338-347.
30. H. B. Huntington, A. R. Grone; *J. Phys. Chem. Solids*, Vol. 20, Nos. 1/2 (1961), p. 76-87.
31. I. A. Blech, E. S. Meieran; *Appl. Phys. Letters*, Vol. 11, No.8 (1967), p. 263-266.
32. M. J. Attardo, R. Rosenberg; *J. Appl. Phys.*, Vol. 41, No.6 (1970), p. 2381-2386.

33. J. D. Venables, R. G. Lye; Proc. Annual Reliability Phys. Symp., 10th (1972), p. 159-164.
34. R. Rosenberg, M. Ohring; J. Appl. Phys., Vol. 42, No. 13 (1971) p. 5671-5679.
35. J. R. Black; Proc. IEEE, Vol. 57, No. 9 (1969), p. 1587-1594.
36. F. M. D'Heurle, Proc. IEEE, Vol. 59, No. 10 (1971), p. 1409-1418.
37. G. Hass, M. H. Francombe, R. W. Hoffman; "Physics of Thin Films," Academic Press, Vol. 7 (1973), p. 257.
38. "Handbook of Chemistry and Physics," 53rd Ed., CRC Press (1972-1973).
39. J. M. Blakely; "Introduction to the Properties of Crystal Surfaces," Pergamon Press (1973), Chap. 1.
40. V. H. Schenck, M. G. Froberg and K. Hoffmann; Archiv für das Eisenhüttenwesen (1963), p. 93-100.